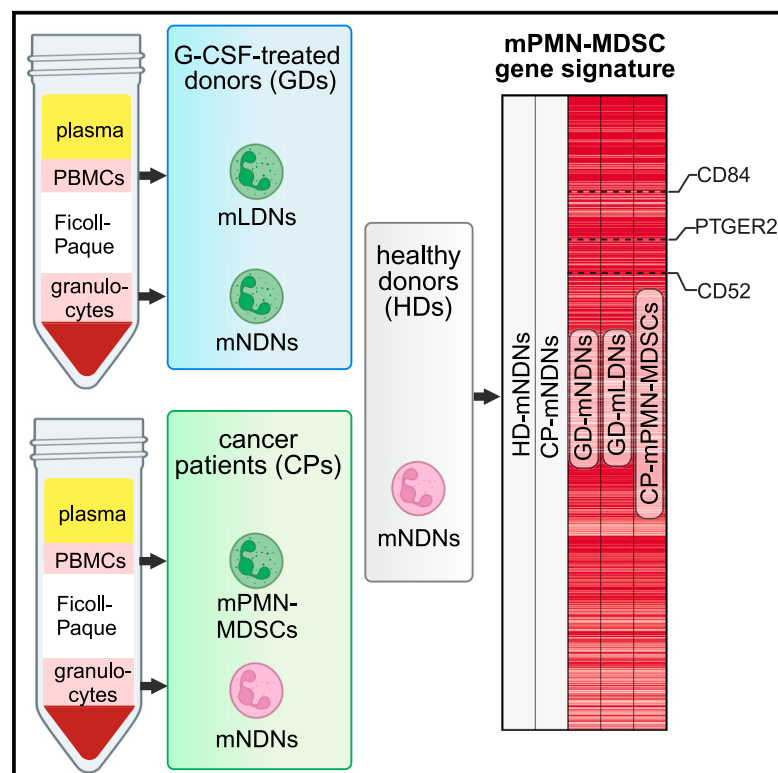


# Surface CD52, CD84, and PTGER2 mark mature PMN-MDSCs from cancer patients and G-CSF-treated donors

## Graphical abstract



## Authors

Francesca Pettinella, Barbara Mariotti, Chiara Lattanzi, ..., Sven Brandau, Marco A. Cassatella, Patrizia Scapini

## Correspondence

marco.cassatella@univr.it (M.A.C.), patrizia.scapini@univr.it (P.S.)

## In brief

Pettinella et al. show that mature PMN-MDSCs from cancer patients and G-CSF-treated donors share a distinct gene signature, including transcripts related to their immunosuppressive nature. Analysis of such a gene signature led to recognition of markers of mature PMN-MDSCs, helpful for their identification and immuno-monitoring; namely, CD52, CD84, and PTGER2.

## Highlights

- Mature PMN-MDSCs from cancer and G-CSF-treated donors share common gene signature
- Mature PMN-MDSCs distinctively express CD52, CD84, and PTGER2
- Mature suppressive neutrophils from G-CSF-treated donors represent reliable PMN-MDSCs



## Article

# Surface CD52, CD84, and PTGER2 mark mature PMN-MDSCs from cancer patients and G-CSF-treated donors

Francesca Pettinella,<sup>1,12</sup> Barbara Mariotti,<sup>1,12</sup> Chiara Lattanzi,<sup>1,12</sup> Kirsten Bruderek,<sup>2</sup> Marta Donini,<sup>1</sup> Sara Costa,<sup>1</sup> Olivia Marini,<sup>1</sup> Giulia Iannoto,<sup>1</sup> Sara Gasperini,<sup>1</sup> Elena Cavegion,<sup>1</sup> Monica Castellucci,<sup>3</sup> Federica Calzetti,<sup>1</sup> Francisco Bianchetto-Aguilera,<sup>1</sup> Elisa Gardiman,<sup>1</sup> Matteo Giani,<sup>1</sup> Stefano Dusi,<sup>1</sup> Maurizio Cantini,<sup>4</sup> Aurora Vassanelli,<sup>4</sup> Denise Pavone,<sup>4</sup> Michele Milella,<sup>5</sup> Sara Pilotto,<sup>5</sup> Pamela Biondani,<sup>6</sup> Benedikt Höing,<sup>7</sup> Marie Carolin Schleupner,<sup>7</sup> Timon Hussain,<sup>7</sup> Boris Hadaschik,<sup>8</sup> Cordelia Kaspar,<sup>8</sup> Carlo Visco,<sup>9</sup> Cristina Tecchio,<sup>9</sup> Leo Koenderman,<sup>10</sup> Flavia Bazzoni,<sup>1</sup> Nicola Tamassia,<sup>1</sup> Sven Brandau,<sup>2,11</sup> Marco A. Cassatella,<sup>1,\*</sup> and Patrizia Scapini<sup>1,13,\*</sup>

<sup>1</sup>Section of General Pathology, Department of Medicine, University of Verona, 37134 Verona, Italy

<sup>2</sup>Research Division, Department of Otorhinolaryngology, University Hospital Essen, 45122 Essen, Germany

<sup>3</sup>Centro Piattaforme Tecnologiche, University of Verona, Verona, Italy

<sup>4</sup>Transfusion Medicine Department, University and Hospital Trust (AOUI), Verona, Italy

<sup>5</sup>Section of Innovation Biomedicine – Oncology Area, Department of Engineering for Innovation Medicine (DIMI), University of Verona, Verona, Italy

<sup>6</sup>Section of Oncology, University and Hospital Trust (AOUI) of Verona, Verona, Italy

<sup>7</sup>Department of Otorhinolaryngology, University Hospital Essen, Essen, Germany

<sup>8</sup>Department of Urology, University Hospital Essen, Essen, Germany

<sup>9</sup>Section of Hematology and Bone Marrow Transplant Unit, Department of Engineering for Innovation Medicine (DIMI), University of Verona, Verona, Italy

<sup>10</sup>Department of Respiratory Medicine and Center for Translational Immunology, University Medical Center Utrecht, 3584CX Utrecht, the Netherlands

<sup>11</sup>German Cancer Consortium, Partner Site Essen-Düsseldorf, Essen, Germany

<sup>12</sup>These authors contributed equally

<sup>13</sup>Lead contact

\*Correspondence: marco.cassatella@univr.it (M.A.C.), patrizia.scapini@univr.it (P.S.)

<https://doi.org/10.1016/j.xcrm.2023.101380>

## SUMMARY

Precise molecular characterization of circulating polymorphonuclear myeloid-derived suppressor cells (PMN-MDSCs) is hampered by their mixed composition of mature and immature cells and lack of specific markers. Here, we focus on mature CD66b<sup>+</sup>CD10<sup>+</sup>CD16<sup>+</sup>CD11b<sup>+</sup> PMN-MDSCs (mPMN-MDSCs) from either cancer patients or healthy donors receiving G-CSF for stem cell mobilization (GDs). By RNA sequencing (RNA-seq) experiments, we report the identification of a distinct gene signature shared by the different mPMN-MDSC populations under investigation, also validated in mPMN-MDSCs from GDs and tumor-associated neutrophils (TANs) by single-cell RNA-seq (scRNA-seq) experiments. Analysis of such a gene signature uncovers a specific transcriptional program associated with mPMN-MDSC differentiation and allows us to identify that, in patients with either solid or hematologic tumors and in GDs, CD52, CD84, and prostaglandin E receptor 2 (PTGER2) represent potential mPMN-MDSC-associated markers. Altogether, our findings indicate that mature PMN-MDSCs distinctively undergo specific reprogramming during differentiation and lay the groundwork for selective immunomonitoring, and eventually targeting, of mature PMN-MDSCs.

## INTRODUCTION

Low-density neutrophils (LDNs) consist of CD66b<sup>+</sup>/CD15<sup>+</sup> neutrophils/neutrophil-like cells that, because of their altered buoyancy, typically accumulate within the PBMC fraction after density gradient centrifugation of blood.<sup>1–3</sup> While LDNs isolated from the peripheral blood of patients with autoimmune diseases display proinflammatory activities and are known as low-density granulocytes (LDGs),<sup>4</sup> LDNs isolated from the peripheral blood of cancer

patients, pregnant women, or patients with infectious diseases have immunosuppressive functions and are called polymorphonuclear myeloid-derived suppressor cells (PMN-MDSCs).<sup>2,5–7</sup>

It is, however, impossible to selectively immunomonitor PMN-MDSCs because, at least based on their putative CD66b<sup>+</sup>CD15<sup>+</sup>CD14<sup>–/dim</sup>CD33<sup>dim</sup>HLA-DR<sup>–</sup> phenotype,<sup>8</sup> they do not differ from non-immunosuppressive normal density neutrophils (NDNs) or even from proinflammatory LDGs.<sup>9,10</sup> Moreover, precise knowledge of the molecular and phenotypic features of PMN-MDSCs



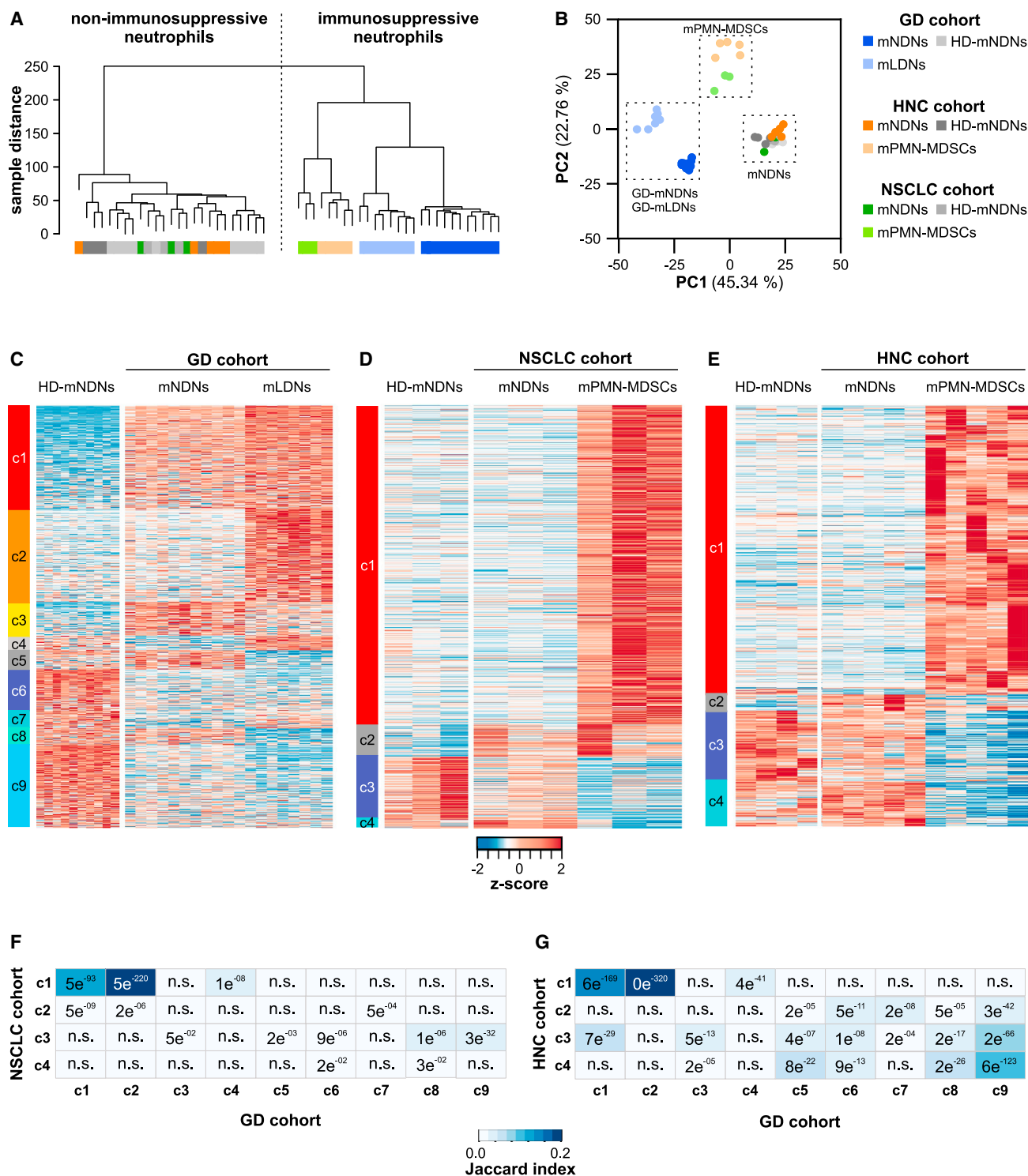


**Figure 1. mNDNs and mLDNs from GDs display transcriptomic similarities to mPMN-MDSCs from NSCLC and HNC patients**

Circulating mLDNs and mNDNs from GDs (n = 8–11), mPMN-MDSCs and autologous mNDNs from NSCLC (n = 3) and HNC patients (n = 5), as well as group-related control mNDNs from HDs (n = 10 for GDs; n = 3 and n = 4 for NSCLC and HNC patients, respectively) were isolated and subjected to RNA-seq experiments.

(A) Dendrogram of the unsupervised hierarchical clustering analysis based on the top 500 highly variable genes among the GD, NSCLC, and HNC cellular sample cohorts.

(legend continued on next page)

is also hampered by the fact that they consist of mixtures of mature and immature neutrophils (with the latter including mostly band cells and metamyelocytes but also a few myelocytes and promyelocytes).<sup>11</sup> In this context, we recently demonstrated that both mature CD66b<sup>+</sup>CD10<sup>+</sup>CD11b<sup>high</sup>CD16<sup>high</sup> NDNs and CD66b<sup>+</sup>CD10<sup>+</sup>CD11b<sup>high</sup>CD16<sup>high</sup> LDNs from healthy subjects receiving G-CSF for stem cell mobilization (hereafter called mNDNs and mLDNs from GDs, respectively), but not immature CD66b<sup>+</sup>CD10<sup>−</sup>CD11b<sup>+/−</sup>CD16<sup>+/−</sup> LDNs (iLDNs from GDs), manifest potent PMN-MDSC-like functions.<sup>12</sup> Although our findings were in contrast with the assumption that immunosuppressive PMN-MDSCs are largely in an immature differentiation state,<sup>6,13</sup> they have been subsequently substantiated by other studies on mature PMN-MDSCs (mPMN-MDSCs) from the peripheral blood of patients with head and neck cancer (HNC)<sup>14</sup> and urological cancer (UC)<sup>14</sup> or on mature neutrophils from the bone marrow (BM) of multiple myeloma patients.<sup>15</sup> However, several issues need to be clarified; for instance, whether specific molecular features and/or distinct markers exist for mPMN-MDSCs, whether mPMN-MDSCs represent a neutrophil population that is reprogrammed during differentiation, or whether they are instead generated from preexisting mature neutrophils.

With the purpose of identifying reliable markers of circulating mPMN-MDSCs, here we report the identification of a distinct gene signature shared by mPMN-MDSCs from cancer patients and GDs consisting of transcripts that clearly reflect their immunosuppressive/protumor features as well as their maturation reprogramming. Notably, such mPMN-MDSC gene signature led us to also uncover surface molecules markedly upregulated on circulating human mPMN-MDSCs; namely CD52, CD84, and prostaglandin E receptor 2 (PTGER2).

## RESULTS

### Identification of a gene signature shared by mPMN-MDSCs from NSCLC and HNC patients and mNDNs/mLDNs from GDs

Initial experiments confirmed that both mNDNs and mLDNs from GDs not only exert immunosuppressive functions toward T cells (Figure S1A) but also display a significant capacity to inhibit natural killer (NK) cell-mediated tumor cell cytotoxicity (Figure S1B) as well as reduced cytotoxic activity toward K562 cells (Figure S1C)<sup>12,16,17</sup> at substantially similar levels. Because these data further validated both mNDNs and mLDNs from GDs as functional PMN-MDSC-like cells,<sup>6</sup> we then investigated whether they also share a “gene signature” with cancer mPMN-MDSCs. Thus, we compared the transcriptomes of mNDNs and mLDNs from GDs with those of mPMN-MDSCs from HNC and NSCLC patients, using mNDNs from HDs of each cohort as controls.

Figures S2A–S2C show the gating strategies utilized to isolate all of the different mature CD66b<sup>+</sup>CD10<sup>+</sup>CD11b<sup>high</sup>CD16<sup>high</sup> neutrophil/PMN-MDSC populations. As shown in Figure 1A, hierarchical clustering analysis of the 500 most variable genes uncovered that, consistent with their immunosuppressive capacity,<sup>12,14</sup> both mNDNs and mLDNs from GDs clustered with mPMN-MDSCs from NSCLC and HNC patients, being distinct from control mNDNs isolated from either HDs or cancer patients. Moreover, principal component analysis (PCA; Figure 1B) further demonstrated that (1) mPMN-MDSCs from NSCLC and HNC patients cluster together despite their different tumor origin and clearly segregate from both their autologous mNDNs and their group-related mNDNs from HDs, (2) mNDNs and mLDNs from GDs form two distinct but close clusters that markedly separate from both group-related mNDNs from HDs, (3) mNDNs from cancer patients cluster with all other mNDNs from HDs, and (4) cellular sample replicates show substantial similarity, thus evidencing distinctive cell identities regardless of the donor origin. All in all, this analysis supported our hypothesis of a shared transcriptional program between mPMN-MDSCs from cancer patients and mNDNs/mLDNs from GDs. Then, by using the likelihood ratio test (LRT) to perform differential gene expression analysis, we identified a total of 7,506 differentially expressed genes (DEGs) among the transcriptomes of mNDNs and mLDNs from GDs and cohort-related mNDNs from HDs (Data S1). By contrast, 1,018 and 5,075 DEGs resulted among the transcriptomes of either mPMN-MDSCs from NSCLC or HNC patients and their autologous mNDNs and group-related mNDNs from HDs, respectively (Data S1). The 7,506 DEGs resulting from the GD cohort were divided into 9 clusters according to K-means clustering analysis (cluster 1 [c1]–c9; Figure 1C). Interestingly, seven of these clusters (corresponding to 92% of the DEGs) showed a concordant gene modulation (namely, of upregulated genes for c1, c2, and c3 and of downregulated genes for c6–c9), while only two clusters displayed a discordant gene modulation (namely, c4 and c5, corresponding to only 8% of the DEGs), in both mNDNs and mLDNs from GDs (Figure 1C). For the DEGs identified in cancer mPMN-MDSCs, K-means clustering analysis instead uncovered 4 clusters for each cohort (c1–c4), with the largest being c1 (corresponding to either 75% or 79% of the total DEGs of the NSCLC or HNC cohort, respectively), exclusively composed of upregulated genes (Figures 1D and 1E). By calculating the Jaccard index among all GD and either NSCLC clusters (Figure 1F) or HNC clusters (Figure 1G), we found that the most significant similarities occurred among c1 and c2 of mNDNs/mLDNs from GDs altogether (which account for 85% of their total commonly upregulated DEGs; Figure 1C) and c1 of mPMN-MDSCs from both NSCLC and HNC patients (Figures 1D and 1E).

(B) PCA scatterplot of the top 500 highly variable genes.

(C–E) Heatmaps displaying the expression patterns of DEGs identified by comparing GD (C), NSCLC (D), and HNC (E) mPMN-MDSC sample cohorts and group-related mNDNs from HDs. Data are shown as Z-scaled fragment per kilobase of transcript per million mapped reads (FPKM) values (Z score), while the clusters obtained by K-means clustering are reported on the left of each heatmap.

(F and G) Heatmaps displaying the Jaccard similarity index, illustrating the extent of the overlap among the DEG clusters identified in mNDNs/mLDNs from GDs (GD cohort) and those of mPMN-MDSCs from NSCLC (F) or HNC (G) patients (NSCLC and HNC cohort, respectively). Box colors correlate with the Jaccard score value according to the Jaccard index scale, while box numbers indicate the p value for each comparison according to Fisher's exact test.

See also Figure S2 and Data S1.



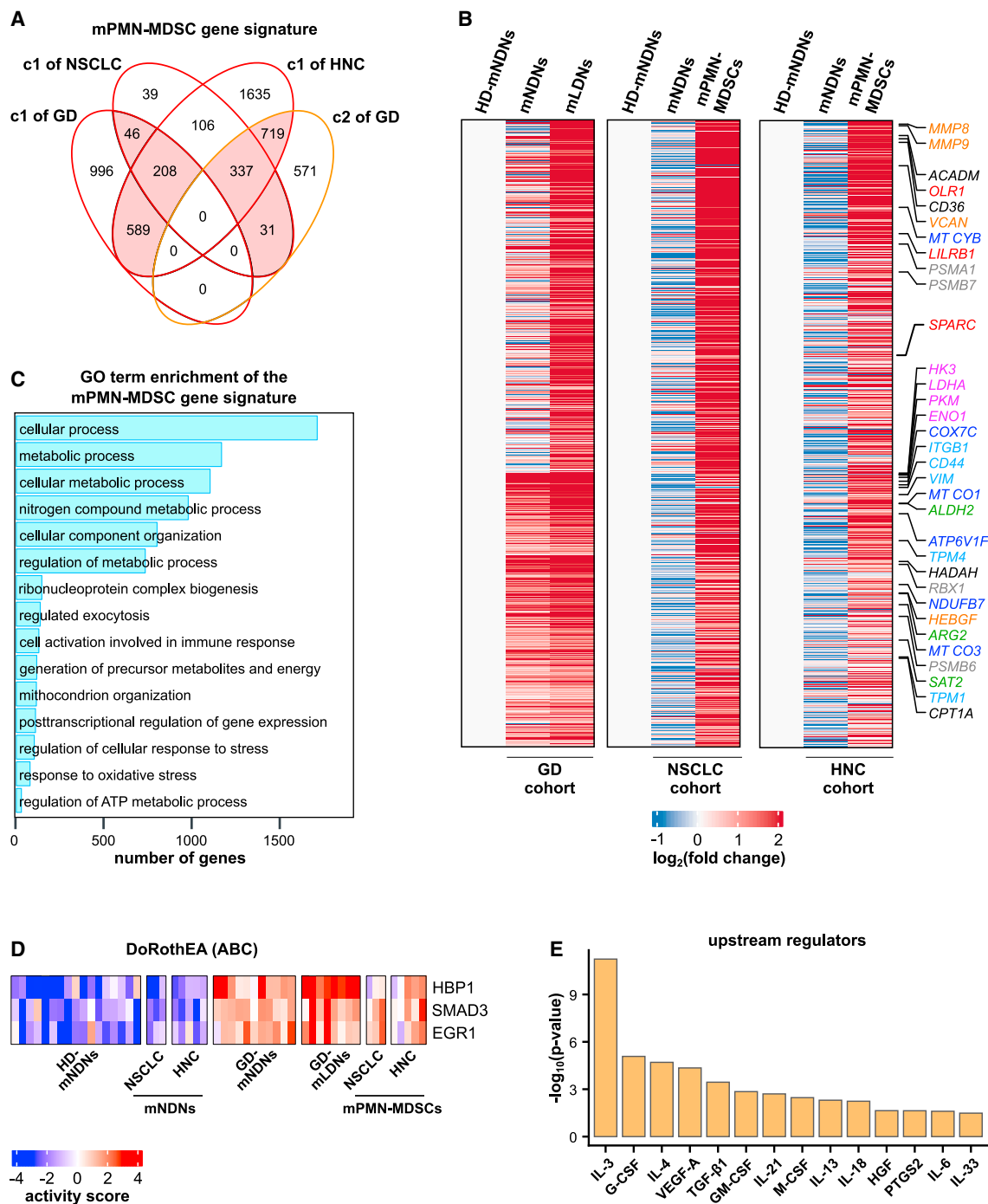


**Figure 2. Identification and characterization of a gene signature and associated TF regulons and upstream regulators shared by mPMN-MDSCs from NSCLC and HNC patients and mNDNs/mLDNs from GDs**

(A) Venn diagram showing the genes shared between cluster 1 (c1) and c2 of the GD cellular sample cohort and c1 of NSCLC and/or HNC cellular sample cohorts. Intersections highlighted in pink were selected for the generation of the mPMN-MDSC gene signature.

(B) Heatmaps displaying the expression of the genes included in the mPMN-MDSC gene signature in either mNDNs/mLDNs from GDs (left), or mPMN-MDSCs from NSCLC (center) or HNC (right) patients. Data are represented as log<sub>2</sub> (fold change) relative to the mNDNs from HDs. Selected genes are listed on the right of the heatmap; font colors mean that they are included in the following biological process: black, metabolism; green, arginine and proline metabolism; blue, ATP metabolism; gray, hypoxia; purple, glycolysis; orange, pro-angiogenic; light blue, EMT; red, PMN-MDSC-associated genes from the literature.

(legend continued on next page)

Identification of the genes belonging to these selected clusters resulted in a total of 1,930 DEGs commonly upregulated in mPMN-MDSCs from NSCLC and/or HNC patients and mNDNs/mLNs from GDs (Figure 2A, pink intersections; Data S2), which were all together defined as “mPMN-MDSC gene signature” (see heatmap in Figure 2B). By Gene Ontology (GO) term enrichment analysis, the mPMN-MDSC gene signature was found to be associated with several biological processes, such as metabolic processes and response to oxidative stress, typically characterizing cancer-associated myeloid cells (Figure 2C). Specifically, genes associated with processes such as “arginine and proline metabolism” (i.e., *ALDH2*, *ARG2*, and *SAT2*), “fatty acid and lipoprotein metabolism” (i.e., *ACADM*, *HADHA*, *CD36*, and *CPT1A*), “oxidative phosphorylation and energy (ATP) metabolism” (i.e., *ATP6V1F*, *COX7C*, *MT-CO3*, *MT-CO1*, *MT-CYB*, and *NDUFB7*), “cell response to hypoxia” (i.e., *PSMB6*, *PSMB7*, *RBX1*, and *PSMA1*), and “glycolysis” (i.e., *PKM*, *ENO1*, *HK3*, and *LDHA*) were found to be included in the mPMN-MDSC gene signature (Figure 2B). Notably, the defined signature also included genes previously proposed as being PMN-MDSC associated, such as *LIRB1*,<sup>18</sup> *OLR1/LOX1*,<sup>19</sup> and *SPARC*<sup>20</sup> (Figure 2B), or typically associated with tumor progression, including genes favoring angiogenesis, such as *MMP8*, *MMP9*, *HBEGF*, and *VCAN*, or regulating the epithelial-mesenchymal transition (EMT), such as *VIM*, *TPM1*, *TPM4*, *CD44*, and *ITGB1*.

To assess the existence of eventual specific transcriptional regulatory networks associated with our defined mPMN-MDSC gene signature, we used DoRothEA, a recently developed software that estimates transcription factor (TF) activities.<sup>21</sup> By applying the statistical framework VIPER<sup>22</sup> to the upregulated genes belonging to the mPMN-MDSC gene signature, we identified the top 25 TF regulons (data not shown); among them, HBP1, SMAD3, and EGR1 were more consistently represented across all replicates of our mPMN-MDSC samples (Figure 2D).

Finally, we performed Ingenuity Pathway Analysis (IPA) of the DEGs included in the mPMN-MDSC gene signature to identify predicted upstream regulators common to mPMN-MDSCs from NSCLC and/or HNC patients and mNDNs/mLNs from GDs (Figure 2E). Besides G-CSF, several other growth factors (such as GM-CSF and transforming growth factor  $\beta$ 1 [TGF- $\beta$ 1]), cytokines (such as interleukin-3 [IL-3], IL-6, IL-4, and IL-13), and enzymes involved in prostanoid production (such as PTGS2) emerged as mediators potentially able to induce mPMN-MDSC gene signature expression in mPMN-MDSCs from our different models (Figure 2E).

Altogether, these analyses led us to uncover a gene signature and associated top TF regulons shared by mPMN-MDSCs from NSCLC and/or HNC patients and mNDNs/mLNs from GDs that reflect their immunosuppressive/protumor features and reprogramming.

### Enrichment of the mPMN-MDSC gene signature in tumor-associated neutrophils (TANs) from NSCLC patients and mNDNs/mLNs from GDs examined by single-cell RNA sequencing (scRNA-seq) experiments

The capacity to truly generate neutrophils with functional PMN-MDSC activities *in vitro* is doubtful.<sup>12,13,23–27</sup> In this context, the results shown in Figure 2E show that the mPMN-MDSC gene signature appears to be driven by a complex regulatory network of mediators likely present in tumor-like microenvironments. Nonetheless, we investigated whether the mPMN-MDSC gene signature could be induced in mature neutrophils from HDs incubated *in vitro* with agonists previously proposed to induce suppressive functions.<sup>13,23–27</sup> With all of the limits of this approach, only minor fractions of the mPMN-MDSC gene signature were found to be induced in HD neutrophils incubated with G-CSF, GM-CSF, LPS, or R848 (Figure S3A; Data S3). On the other hand, the mPMN-MDSC gene signature was found to be significantly enriched in previously reported gene signatures obtained by bulk RNA-seq experiments of either unfractionated PMN-MDSCs (i.e., mature and immature PMN-MDSCs) from HNC and NSCLC patients<sup>19</sup> or total mature neutrophils from the BM of multiple myeloma patients<sup>15</sup> (improperly defined as PMN-MDSCs) (Figure 3A; Data S3). By contrast, it resulted very poorly represented either in previously published transcriptomes of proinflammatory mLDGs from patients with systemic lupus erythematosus (SLE)<sup>9</sup> (Figure 3A; Data S3) or in the transcriptome of CD16<sup>high</sup>CD62L<sup>low</sup> suppressive neutrophils isolated from LPS-treated donors (Pillay et al.<sup>28</sup> this study; Figure 3A; Data S3), again obtained by bulk RNA-seq experiments. Moreover, by examining published scRNA-seq datasets,<sup>29,30</sup> we found that our mPMN-MDSC gene signature is also enriched in the transcriptomes of TANs from NSCLC patients (Figures 3B–3E). Specifically, the datasets related to TANs and normal adjacent tissue-associated neutrophils (NANs) from the large-scale single-cell atlas recently published by Salcher et al.<sup>29</sup> (Figure S3B) and the datasets related to TANs from Zilionis et al.<sup>30</sup> (Figure S3C) were integrated (Figures 3B–3D) and analyzed as described in STAR Methods. Based on the expression levels of the NAN (Figure 3B, left) and TAN (Figure 3B, right) signatures,<sup>29</sup> we were then able to identify “NAN-like cells” and “TAN-like cells” in each datasets (colored green and violet, respectively, in Figures 3C, S3B, and S3C). Notably, the most tumor-specific TAN cluster reported in the study by Zilionis et al.,<sup>30</sup> hN5 (Figure S3C), resulted as the cluster with the highest score enrichment of the mPMN-MDSC gene signature (Figure S3D). Moreover, by calculating the enrichment score of the mPMN-MDSC gene signature in each single cell shown in Figure 3C, we found that TAN-like cells displayed the highest score (Figures 3D and 3E).

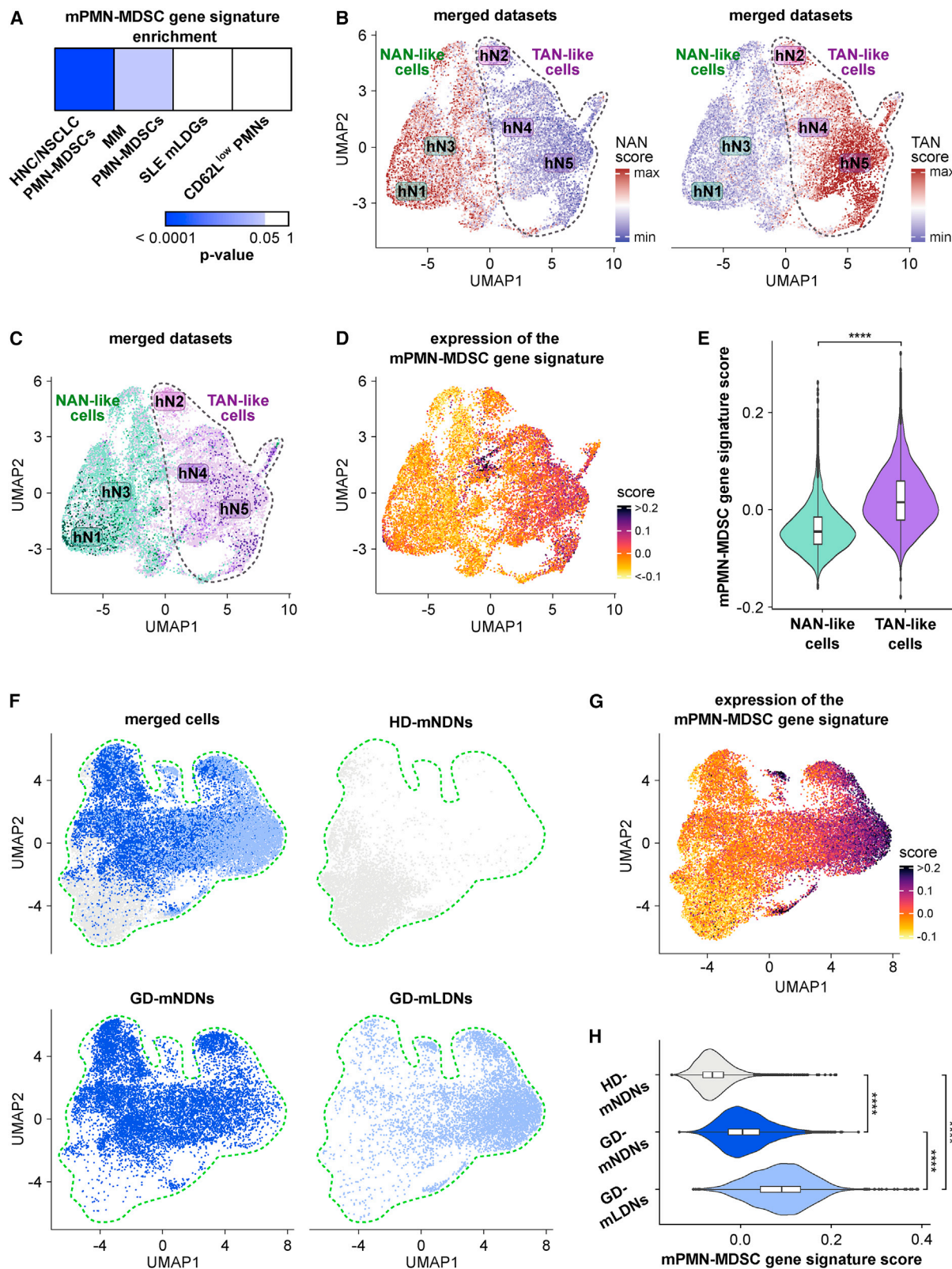
To further validate the reproducibility of our mPMN-MDSC gene signature, we performed scRNA-seq experiments using

(C) Graph depicting the GO terms significantly (false discovery rate [FDR] < 0.05) over-represented in the mPMN-MDSC gene signature. Bars indicate the number of genes composing the top 15 enriched GO terms.

(D) Heatmap displaying the activity score of the most consistently active TF regulons across all replicates of our GD and cancer cellular samples, as inferred using DoRothEA by applying the statistical framework VIPER to the mPMN-MDSC gene signature.

(E) Graph showing the most significant upstream regulators of mPMN-MDSC gene signature expression in mPMN-MDSCs from HNC and NSCLC patients and GDs, as revealed by IPA. The bars indicate the p value on a logarithmic scale according to Fisher's exact test.

See also Figure S3 and Data S2.



(legend on next page)

whole CD66b<sup>+</sup> neutrophils sorted from the NDN and LDN fractions of GDs and the NDN fraction of HDs as controls. After normalization and filtering, our datasets included transcriptomes from total NDNs from HDs (6,070 cells) (Figure S3E) and merged NDNs/LDNs from GDs (23,453 cells) (Figure S3F). We then selected only the most mature cells for further analysis (namely, 10,339 mNDNs and 6,393 mLDNs from GDs and 6,070 mNDNs from HDs; Figures S3E and S3F, green gates; Figure 3F), based on the expression levels of a transcriptional module previously associated with neutrophils at their later stage of differentiation (i.e., cluster r2 of Figure 1 in Grassi et al.<sup>31</sup>). Single-cell transcriptomes of mature HD and GD neutrophils were then merged and visualized in a UMAP plot (Figure 3F, top left). UMAP data confirmed the closer similarity of mNDNs from GDs to autologous mLDNs rather than to mNDNs from HDs, as also observed by bulk RNA-seq (Figures 1A–1C). In fact, mNDNs from HDs (Figure 3F, top right) were found clearly separate from mNDNs (Figure 3F, bottom left) and mLDNs (Figure 3F, bottom right) from GDs, the latter two populations being instead substantially overlapped (see the central/right regions of the UMAP plot in Figure 3F). By calculating the enrichment score of the mPMN-MDSC gene signature in each single cell shown in Figure 3F, we found that the highest scores were displayed by mLDNs from GDs (Figures 3G and 3H), while, compared with mNDNs from HDs, a significant score was also displayed by mNDNs from GDs (Figures 3G and 3H).

We also characterized a short gene signature deriving from the 545 commonly upregulated DEGs that are simultaneously shared in all 3 models (208 genes shared by c1 of NSCLC, HNC, and GD cells and 337 genes shared by c1 of HNC and NSCLC and c2 of GD cells) (Figure S3G). This analysis was performed to exclude the possibility that G-CSF-dependent genes are overrepresented in the signature. We found that such a short mPMN-MDSC gene signature, similar to the more comprehensive mPMN-MDSC gene signature (Figure 3), resulted significantly enriched in published TAN signatures<sup>29,30</sup> (Figure S3H) and in our scRNA-seq GD mLDN/mNDN datasets (Figure S3I) as well as poorly enriched in proinflammatory mLDGs from SLE patients<sup>9</sup> (Figure S3J) or in the transcriptome of CD16<sup>high</sup>CD62L<sup>low</sup> suppressive neutrophils isolated from LPS-treated donors<sup>28</sup> (Figure S3J). However, the short mPMN-MDSC gene signature resulted enriched only in

one of the two published PMN-MDSC signatures (Figure S3J) and contained fewer genes related to biological processes associated with PMN-MDSCs (Figure S3K) than the more comprehensive mPMN-MDSC gene signature (Figure 2B). Therefore, we continued our studies using the more comprehensive mPMN-MDSC gene signature shown in Figures 2A and 2B because it better reflects the complex mPMN-MDSC transcriptional reprogramming in tumor-like environments.

In summary, our data demonstrate that the identified, more comprehensive mPMN-MDSC gene signature clearly distinguishes mPMN-MDSCs not only from proinflammatory mLDGs but also from other types of mature neutrophil populations shown previously to display suppressive functions. Furthermore, data from our scRNA-seq experiments integrated with those from other studies prove that the mPMN-MDSC signature is significantly expressed, even if at different levels, not only in mPMN-MDSCs from GDs but also in TANs of NSCLC patients.

### Expression of the mPMN-MDSC gene signature in neutrophil progenitors

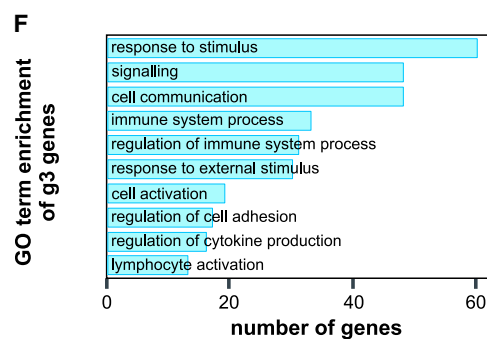
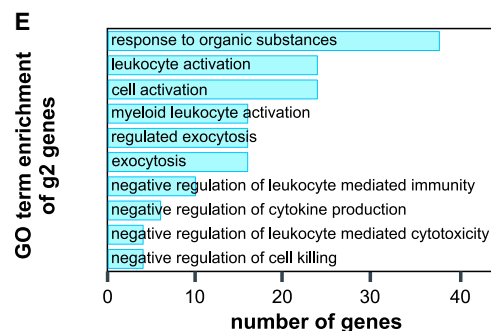
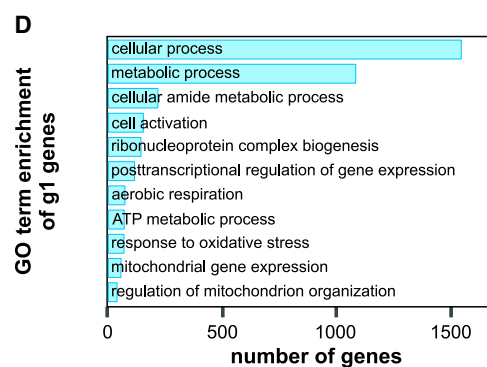
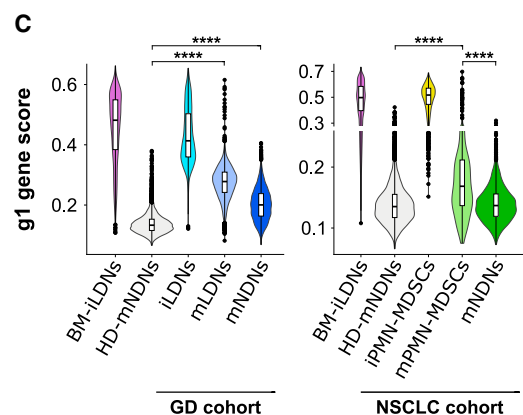
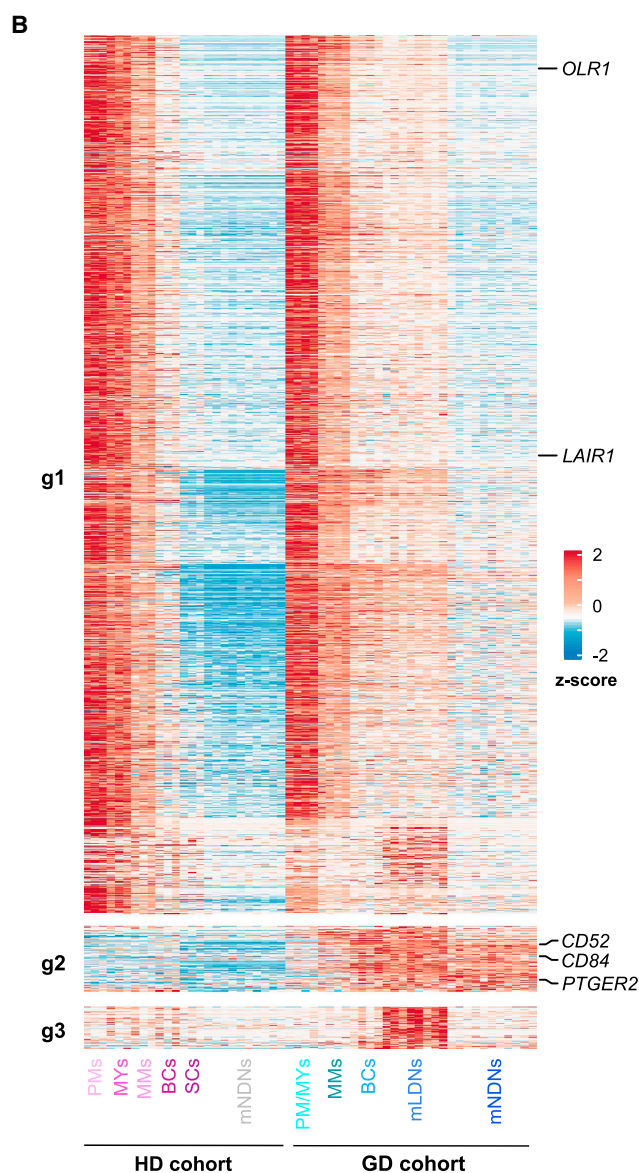
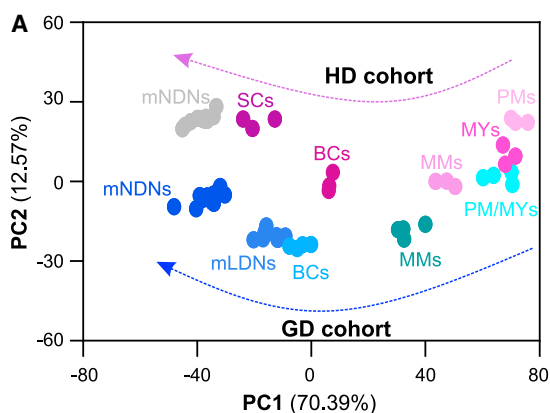
To clarify whether and at which stage of neutrophil differentiation the mPMN-MDSC gene signature is recognizable, we used cells from GDs. Hence, in addition to mNDNs and mLDNs, we sorted from LDNs and profiled by RNA-seq (1) CD66b<sup>+</sup>CD10<sup>−</sup>CD11b<sup>+</sup>CD16<sup>+</sup> band cells (BCs), (2) CD66b<sup>+</sup>CD10<sup>−</sup>CD11b<sup>+</sup>CD16<sup>dim</sup> metamyelocytes (MMs), and (3), to recover sufficient cells, CD66b<sup>+</sup>CD10<sup>−</sup>CD11b<sup>dim</sup>CD16<sup>−</sup> myelocytes (MYs) together with CD66b<sup>+</sup>CD10<sup>−</sup>CD11b<sup>−</sup>CD16<sup>−</sup> promyelocytes (PMs) (Figure S2D, top). As reference cells, we RNA-seq profiled PMs, MYs, MMs, BCs, and segmented cells (SCs) from BM aspirates from HDs (Figure S2D, center and bottom). PCA derived from the 500 most variable genes highlighted that the maturation trajectories of neutrophil precursors from GDs (Figure 4A, blue arrow) and HDs (Figure 4A, pink arrow) distribute along similar trends, even though they clearly diverge along PC2 after the MM maturation stage. Then, after overlapping the mPMN-MDSC gene signature with the transcriptomes of immature and mature neutrophils from either peripheral blood from GDs or BM aspirates from HDs, we could identify three major gene groups by K-means clustering analysis; namely, group 1 [g1],

**Figure 3. The mPMN-MDSC gene signature is enriched in published signatures obtained by bulk RNA-seq of various PMN-MDSCs and by scRNA-seq of TANs from NSCLC patients and mNDNs/mLDNs from GDs**

- (A) Enrichment of the mPMN-MDSC gene signature in published gene signatures of PMN-MDSCs<sup>15,19</sup> and mLDGs from SLE (SLE mLDGs<sup>9</sup>) and suppressive CD16<sup>high</sup>CD62L<sup>low</sup> neutrophils (CD62L<sup>low</sup> PMNs) from LPS-treated donors<sup>28</sup> by bulk RNA-seq. Box colors indicate the p value calculated by Fisher's exact test according to the reported scale: white, non-significant enrichment ( $p > 0.05$ ); shades of blue, significant enrichment ( $p < 0.05$ ).
- (B and C) UMAP representations of the integration of the TAN and NAN datasets from Salcher et al.<sup>29</sup> or the TAN dataset from Zilionis et al.<sup>30</sup> For the Zilionis et al.<sup>30</sup> dataset, the TAN clusters defined in the original study (hN1–5)<sup>30</sup> are reported. For every cell, the NAN signature score (B, left) and the TAN signature score (B, right) were calculated by evaluating the expression levels of genes previously found to be highly specific to a NAN or TAN phenotype (i.e., Figure 6H in Salcher et al.<sup>29</sup>). By performing the analysis described in (B), we were able to define two main neutrophil populations defined in this study as NAN-like cells (green) and TAN-like cells (violet) (C) (see also Figures S3B and S3C).
- (D) UMAP plot of the mPMN-MDSC gene signature score, calculated as normalized average expression of the genes composing the signature in each cell.
- (E) Violin plot displaying the mPMN-MDSC gene signature score across the two subsets: NAN-like and TAN-like cells.
- (F) UMAP plot of the neutrophils with a high maturity score (defined as described in Figures S3E and S3F), either merged (top left) or divided by cellular sample cohort: mNDNs from HDs (top right), mNDNs from GDs (bottom left), and mLDNs from GDs (bottom right panel).
- (G) UMAP plot of the mPMN-MDSC gene signature score, calculated as described in (D).
- (H) Violin plot displaying the mPMN-MDSC gene signature score across the different cellular sample cohorts.

\*\*\*\* $p < 0.0001$  by Kruskal-Wallis test followed by pairwise Wilcoxon test. See also Figure S3 and Data S3.





(legend on next page)



g2, and g3 (Figure 4B). More specifically, g1 was found to include 1,720 genes expressed at comparable levels in PMs, MYs, and MMs from both GD and HD cellular samples. Expression of g1 genes, however, was found to be maintained at significantly higher levels in mNDNs and mLDNs from GDs than mNDNs from HDs (Figure 4B), as also revealed by regression analysis (Figure S4A) and confirmed by scRNA-seq experiments (Figure 4C, left). Moreover, scRNA-seq experiments of mature and immature NSCLC PMN-MDSCs revealed that the expression of immature neutrophil genes (g1) is also maintained at higher levels in cancer mPMN-MDSCs than in control autologous or HD mNDNs (Figure 4C, right). These findings thus demonstrate that, similar to mNDNs and mLDNs from GDs, cancer mPMN-MDSCs also display transcriptomic features of their progenitors. The fact that, in GDs, g1 genes appear to be more expressed in mLDNs than in autologous mNDNs (Figure 4B) may explain why the former cells precede the latter ones along their maturation trajectory (Figure 4A). By contrast, g2 was found to include 128 genes that were not only poorly expressed in both HD immature and mature neutrophils, unlike in GD precursors, but also more highly expressed in mature neutrophils from GDs, depending on the gene (Figures 4B and S4B). Finally, g3 was found to include 82 genes that appear to display a higher expression in mLDNs from GDs than in other mature and immature neutrophil populations from GDs and HDs (Figure 4B). GO term enrichment analysis of g1, g2, and g3 genes revealed that most of the biological processes typically attributed to PMN-MDSCs (i.e., metabolic reprogramming, response to oxidative stress, etc.) were enriched in g1 (Figure 4D), while biological processes more specifically related to PMN-MDSC immunosuppressive activities (i.e., cellular activation and exocytosis, negative regulation of leukocyte mediated immunity, etc.) were mostly enriched in g2 (Figure 4E). By contrast, g3 appeared to be enriched in genes more generally associated with immune cell stimulation and signaling than with specific PMN-MDSC features (Figure 4F).

We subsequently investigated whether the mPMN-MDSC gene signature was enriched in the transcriptomes of the four scRNA-seq clusters constituting the most immature precursors of neutrophils described to date; namely, the neutrophil-committed progenitors (NCPs)<sup>32</sup> (Figure S4C). As shown in Figures S4D–S4F, only g1 of the mPMN-MDSC gene signature

was found to be enriched in all four NCP clusters, although at similar levels (Figure S4D) and consistent with its elevated content of immature neutrophil genes. By contrast, neither g2 (Figure S4E) nor g3 (Figure S4F) was found to be enriched in any of the four NCP clusters.

From these experiments, we can conclude that most genes of the mPMN-MDSC gene signature, namely the g1 genes, derive from the maintenance/block of downregulation of transcripts characteristic of normal immature neutrophil precursors that, under physiological conditions, are almost completely downregulated in terminally differentiated neutrophils. Our experiments also highlight that a specific set of genes of the mPMN-MDSC gene signature, namely the g2 genes, is selectively upregulated in PMN-MDSCs/immunosuppressive-committed cells, while g3 genes, whose biological significance remains unclear, are selectively upregulated in mLDNs from GDs only. Furthermore, the fact that either NCPs or more mature neutrophil precursors (i.e., PMs, MYs, MMs, and BCs) do not selectively express the whole mPMN-MDSC signature suggests that, to become mPMN-MDSCs, neutrophils must undergo a specific transcriptional reprogramming along their maturation.

Surface molecules encoded by g2 genes are markedly elevated on mPMN-MDSCs from cancer patients and GDs.

We then focused on g1 and g2 of the mPMN-MDSC gene signature (which both, different from g3, contain genes common to mNDNs and mLDNs from GDs) to examine whether they included genes encoding surface molecules eligible as candidate mPMN-MDSC-associated markers. We started by analyzing g2 genes because they showed the strongest differential expression between HDs and GDs, and we identified 20 mRNAs encoding surface molecules (Data S2), among which we focused on those encoding for CD52 (also known as CDW52, EDDM5, and HE5), CD84 (also known as LY9B and SLAMF5), and PTGER2 (also known as EP2). The choice to look at CD52, CD84, and PTGER2 was also based on their poor expression, at mRNA levels, in mNDNs from HDs compared with mPMN-MDSCs from all models under investigation (as also validated by RT-qPCR; Figures 5A–5C) as well as on the availability of commercial antibodies suitable for flow cytometry analysis. The latter experiments revealed that surface CD52 (Figure 6A, 6D, and 6G), CD84 (Figures 6B, 6E, and 6H), and PTGER2 (Figures 6C, 6F,

**Figure 4. Comparison of mPMN-MDSC gene signature expression between neutrophil precursors from the peripheral blood of GDs and those from BM aspirates of HDs**

RNA-seq experiments with neutrophils at different stages of maturation isolated from BM aspirates from HDs (PM, promyelocyte; MY, myelocyte; MM, metamyelocyte; BC, band cell; SC, segmented cell; n = 3), HD blood (mNDNs, n = 10), or GD blood (PMs/MYs, MMs, BCs, n = 4; mLDNs, n = 8; mNDNs, n = 11) were performed.

(A) PCA plot based on the top 500 variable genes in mature neutrophils and their precursors purified from the peripheral blood of GDs (blue gradations) or the BM (pink gradations) or the peripheral blood (gray) of HDs. Arrows represent the putative maturation trajectories of HD or GD neutrophils.

(B) Heatmap displaying the mRNA expression of the mPMN-MDSC gene signature in neutrophil precursors and mature neutrophils purified from the BM and the peripheral blood of HDs or GDs. Data are shown as Z score (FPKM). The major gene groups (g1–g3) identified by explorative K-means clustering analysis are shown.

(C) Violin plots displaying the score of g1 genes by scRNA-seq data across neutrophils at different maturation stages of the GD (iLDNs, mLDNs, and mNDNs, left) and NSCLC patient (iPMN-MDSCs, mPMN-MDSCs, and mNDNs, right) cohorts. scRNA-seq data of control HD neutrophils at different maturation stages (BM-iLDNs and HD-mNDNs) are also included. The score of g1 genes was determined, in each cell, by calculating the normalized average expression of the genes that compose the g1 group. \*\*\*\*p < 0.0001, by Kruskal-Wallis test followed by pairwise Wilcoxon test.

(D–F) Graphs depicting the top 10 GO terms (FDR < 0.05) significantly enriched in g1 (D), g2 (E), and g3 (F). Bars indicate the number of genes composing the enriched GO terms.

See also Figures S2 and S4.

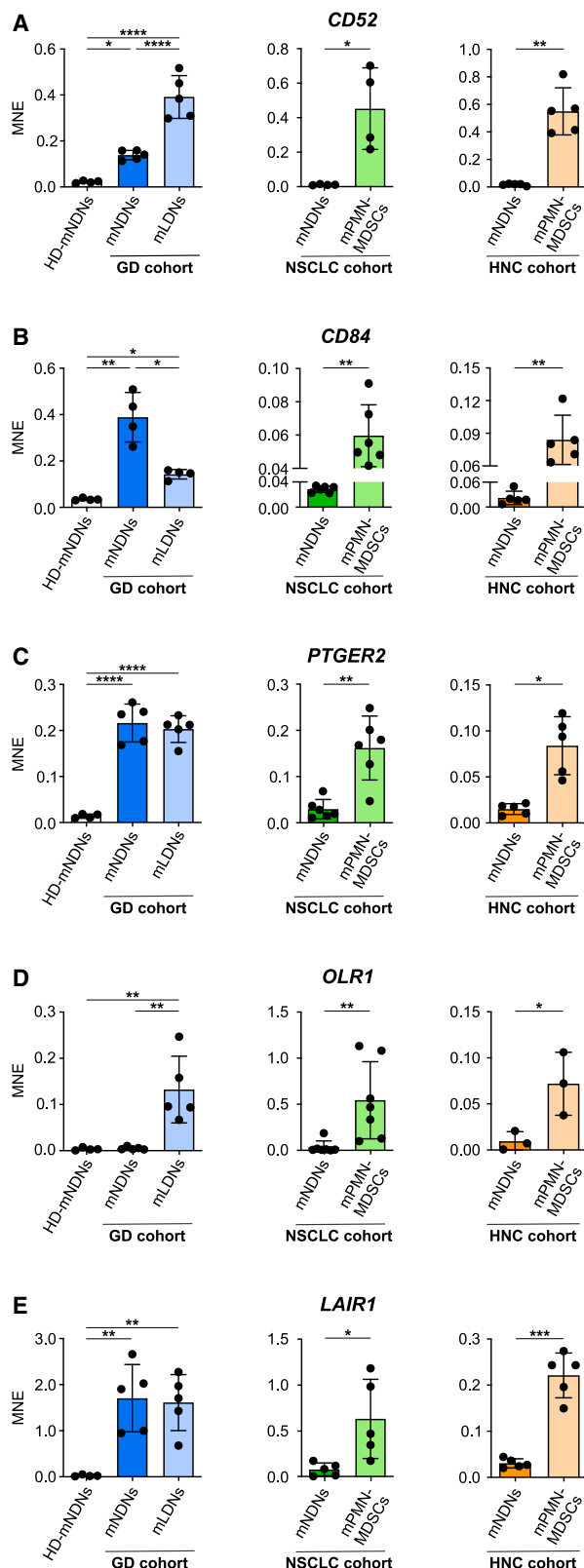


**Figure 5. Expression levels of *CD52*, *CD84*, *PTGER2*, *OLR1*, and *LAIR1* mRNAs in GD, NSCLC, and HNC mPMN-MDSC samples**

Expression levels of *CD52* (A), *CD84* (B), *PTGER2* (C), *OLR1* (D), and *LAIR1* (E) mRNAs in GD (left column of graphs), NSCLC (center column of graphs), and HNC (right column of graphs) cellular samples ( $n = 3-6$ ). Gene expression is depicted as mean normalized expression (MNE) units after normalization to *PPIB* mRNA (mean  $\pm$  SEM). \* $p < 0.05$ , \*\* $p < 0.01$ , \*\*\*\* $p < 0.0001$  by ordinary one-way ANOVA test or Mann-Whitney test.

and 6I) are significantly more elevated on mNDNs/mLDNs from GDs (Figures 6A–6C) and mPMN-MDSCs from either NSCLC (Figures 6D–6F) or HNC (Figures 6G–6I) patients than on group-related mNDNs from HDs or autologous mNDNs, respectively (Figures 6A–6I, S5A, and S5B). Notably, *CD52*, *CD84*, and *PTGER2* expression resulted significantly more elevated also on mPMN-MDSCs from a miscellaneous cohort of patients with DLBCL, RCC, TCC, and breast cancer than on control autologous mNDNs (Figure S6A).

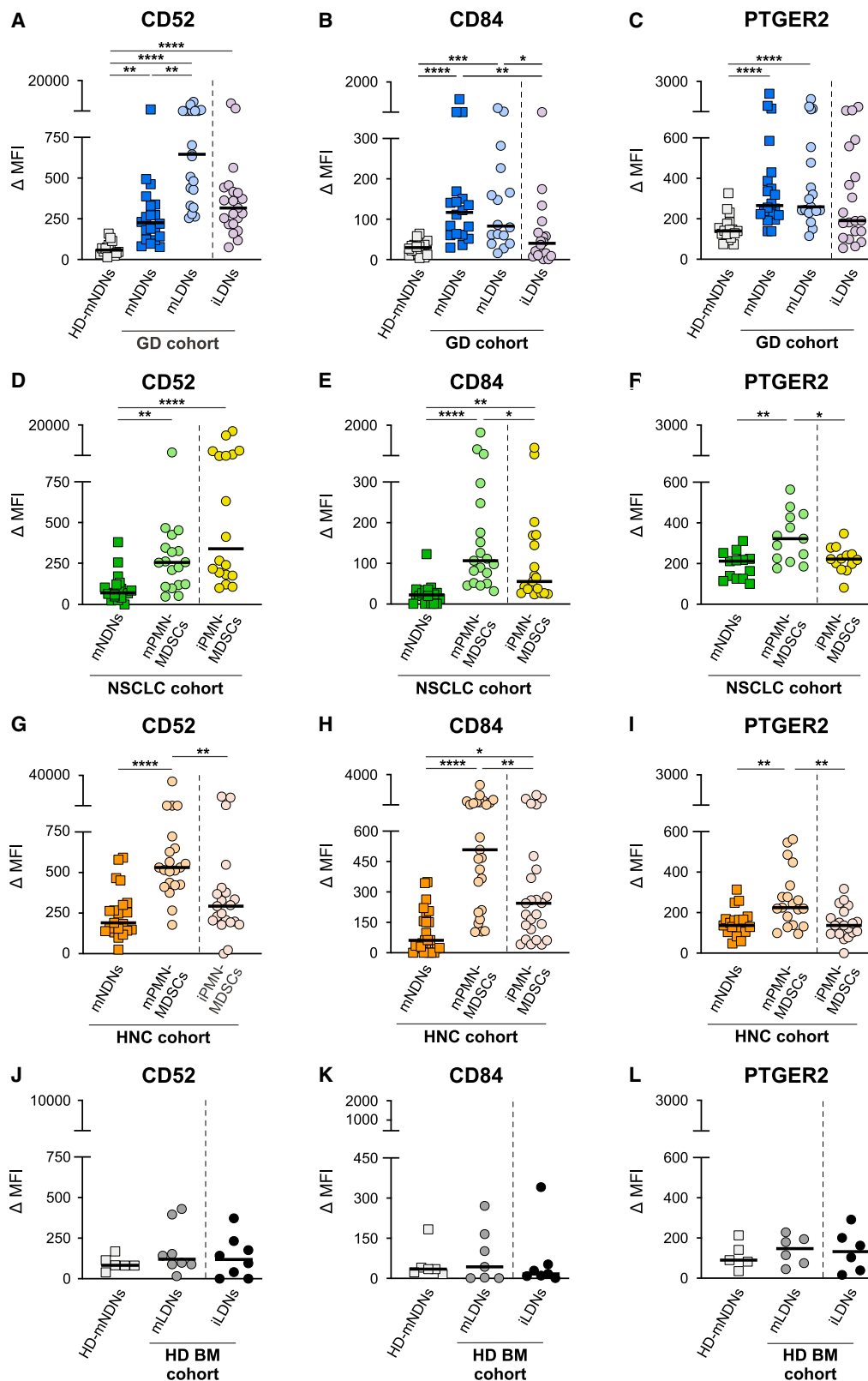
Finally, initial experiments uncovered that, unlike mNDNs from HDs, a larger proportion of mLDNs and mNDNs from GD displayed a *CD52*<sup>+</sup>*CD84*<sup>+</sup>*PTGER2*<sup>+</sup> triple-positive phenotype (Figure S6B).

In a subsequent series of experiments, we also found that all markers (except for *CD52* in NSCLC patients) resulted in overall more elevated (even though not always at significant levels) on mPMN-MDSCs than on autologous either iLDNs from GDs or immature *CD66b*<sup>+</sup>*CD10*<sup>+</sup>*CD11b*<sup>+</sup>*CD16*<sup>+</sup> PMN-MDSCs (iPMN-MDSCs) from cancer patients of the various tumor cohorts tested (Figures 6A–6I and S6A). Finally, *CD52*, *CD84*, and *PTGER2* were found not to be upregulated on mLDNs or on iLDNs from the BM of HDs (Figures 6J–6L). In this context, although we wanted to monitor *CD52*, *CD84*, and *PTGER2* expression in NSCLC and HNC mPMN-MDSCs of patients undergoing different types of therapy, we could not perform these experiments because mPMN-MDSCs were found to dramatically drop (Figures S6C and S6D) independent of the treatment and/or intrinsic patient response.

In summary, these experiments demonstrate that surface *CD52*, *CD84*, and *PTGER2* display stronger expression on PMN-MDSC-committed neutrophils than on normal mature or immature neutrophils, in line with the findings derived from the analysis of the mPMN-MDSC gene signature.

**Lectin-like oxidized low-density lipoprotein receptor (LOX-1) and leukocyte-associated immunoglobulin-like receptor 1 (LAIR-1), two surface molecules encoded by g1 genes, are strongly elevated on immature neutrophils from cancer patients and HDs**

In a final series of experiments, we evaluated the expression of surface molecules encoded by discrete g1 genes. Initially, we focused on *OLR1*, which we confirmed by RT-qPCR to be upregulated in mLDNs, but not in mNDNs from GDs, as well as in mPMN-MDSCs from NSCLC and HNC patients compared with control mNDNs (Figure 5D). *OLR1* encodes for PMN-MDSCs, including for those from NSCLC and HNC patients.<sup>19,33–35</sup> However, total circulating PMN-MDSCs were analyzed in the latter studies,<sup>19,33–35</sup> thus differently from our approach to focus on mPMN-MDSCs only.<sup>12,14</sup> Hence, by doing so, we found that



(legend on next page)

surface LOX-1 is not upregulated on mNDNs/mLNs from GDs (Figure 7A) or on mPMN-MDSCs from NSCLC and HNC cancer patients compared with control mNDNs from HDs or autologous mNDNs (Figures 7C and 7E). By contrast, we found that iPMN-MDSCs from NSCLC and HNC cancer patients (Figures 7C and 7E), but not iLDNs from GDs (Figure 7A), display significantly higher levels of surface LOX-1 than autologous mPMN-MDSCs and/or mNDNs.

Then, we focused on LAIR-1/CD305, an inhibitory receptor known to play an important role in the modulation of immune responses to cancer.<sup>36</sup> By RT-qPCR, we confirmed that LAIR-1/CD305 is strongly upregulated in mNDNs and mLNs from GDs as well as in mPMN-MDSCs from NSCLC and HNC patients compared with control mNDNs (Figure 5E). Although surface LAIR-1 was found significantly more expressed on both mNDNs and mLNs from GDs than on control mNDNs from HDs (Figure 7B), as well as modestly upregulated on mPMN-MDSCs from NSCLC compared with autologous mNDNs (Figure 7D), LAIR-1 was not significantly upregulated on mPMN-MDSCs from HNC patients compared with autologous mNDNs (Figure 7F). Moreover, similar to LOX-1, we found that iLDNs from GDs and iPMN-MDSCs from cancer patients displayed significantly higher LAIR-1 surface levels than mNDNs from HDs (GD cohort; Figure 7B) or autologous mPMN-MDSCs and mNDNs (cancer patient cohorts; Figures 7D and 7F).

Finally, not only iPMN-MDSCs from cancer patients but also iLDNs from the BM of HDs displayed significantly enhanced levels of both surface LOX-1 (Figure 7G) and LAIR-1 (Figure 7H) compared with autologous mLNs or mNDNs from HDs. These observations are consistent with the elevated *OLR1* and *LAIR1* mRNA expression by immature BM neutrophils from HDs (Figure 4B).

In summary, data demonstrate that LOX-1 and LAIR-1 do not specifically mark mPMN-MDSCs because their surface expression is elevated on both iPMN-MDSCs and immature normal neutrophils.

## DISCUSSION

Recent studies from our laboratories have demonstrated that it is the mPMN-MDSCs present in cancer patients and mNDNs/mLNs from GDs that exert the strongest immunosuppressive functions.<sup>12,14</sup> In this research field, an emerging question that remains still unanswered is whether mPMN-MDSCs consist of normal mature neutrophils that have acquired suppressive capacities or instead represent cells that are reprogrammed during differentiation.<sup>6,37–40</sup> Another issue that currently generates confusion is that previous attempts to define gene signatures of

circulating PMN-MDSCs were obtained from either total PMN-MDSC populations (including iLDNs, mLNs, iPMN-MDSCs, and mPMN-MDSCs)<sup>16,19</sup> or total peripheral CD66b<sup>+</sup>/CD15<sup>+</sup> neutrophil populations that consist of NDNs and LDNs altogether.<sup>30,41,42</sup> The only gene signature from presumed mature “PMN-MDSC-like cells” reported to date is that by Perez et al.,<sup>15</sup> however, total BM mature neutrophils from multiple myeloma patients were used in this study and improperly defined as PMN-MDSCs.

In this study, we report the identification of a specific gene signature expressed by mPMN-MDSCs from NSCLC/HNC patients and GDs that clearly reflects their metabolic/functional reprogramming. scRNA-seq experiments further confirmed that the mPMN-MDSC gene signature is significantly enriched not only in both mNDNs/mLNs from GDs but also in published scRNA-seq datasets of TANs from NSCLC patients.<sup>29,30</sup> The latter finding provides evidence of remarkable similarities between human PMN-MDSCs and TANs at the transcriptional level. We also demonstrate that the mPMN-MDSC gene signature is significantly enriched in previous published transcriptomes of PMN-MDSCs/PMN-MDSC-like cells<sup>15,19</sup> but not in transcriptomes of proinflammatory mLDGs from SLE patients<sup>9</sup> or even of CD16<sup>high</sup>CD62L<sup>low</sup> suppressive neutrophils purified from LPS-treated volunteers (Pillay et al.<sup>28</sup> this study). In this context, it should be mentioned that CD16<sup>high</sup>CD62L<sup>low</sup> suppressive neutrophils, similarly to mature neutrophils treated with Toll-like receptor (TLR) agonists *in vitro*,<sup>23</sup> inhibit T cell functions via the release of reactive oxygen species,<sup>28</sup> which is not the mechanism utilized by mPMN-MDSCs from cancer patients<sup>14</sup> or GDs,<sup>12</sup> which instead exert their immunosuppressive activities mainly via arginase release. Accordingly, an enrichment of genes belonging to the arginine and proline metabolism pathways represented features of the mPMN-MDSC gene signature. We also found that the mPMN-MDSC gene signature is not induced in HD neutrophils incubated with stimuli previously shown to induce immunosuppressive capacity *in vitro*, including G-CSFs, GM-CSF, or TLR agonists,<sup>13,23–27</sup> suggesting that *in vivo* differentiated mPMN-MDSCs from cancer patients and GDs are generated via a unique differentiation program. Because about 90% of the signature genes (corresponding to the g1 genes in Figure 4B) were found to be already expressed in BM neutrophil precursors, including NCPs,<sup>32</sup> but not in HD mature neutrophils, we would suggest that mPMN-MDSCs from cancer patients and mNDN/mLNs from GDs consist of a distinct type of mature neutrophils that maintain transcriptomic features of their progenitors due to altered/abnormal differentiation. As revealed by bioinformatics analyses, unique transcriptional regulatory networks were found to be associated with the identified mPMN-MDSC gene signature, in particular HBP1, SMAD3, and EGR1 emerging

### Figure 6. Expression of surface CD52, CD84, and PTGER2 on mPMN-MDSCs and iPMN-MDSC populations from GDs and cancer patients and on mature and immature LDNs from the BM of HDs

Surface CD52 (A, D, G, and J), CD84 (B, E, H, and K), and PTGER2 (C, F, I, and L) expression levels were evaluated by flow cytometry on mNDNs or mLNs/iLDNs from GDs (n = 20) and group-related mNDNs from HDs (n = 17–18) (A–C), mPMN-MDSCs/iPMN-MDSCs and autologous mNDNs from cohorts of patients with NSCLC (D–F, n = 13–19) or HNC (G–I, n = 19–25), and mLNs and iLDNs from BM aspirates from HDs (n = 6–8) or control peripheral blood mNDNs from HDs (HD-mNDNs, n = 5–6) (J–L). Graphs show CD52 (A, D, G, and J), CD84 (B, E, H, and K), and PTGER2 (C, F, I, and L)  $\Delta$  median fluorescence intensity (MFI) values calculated as described in STAR Methods. CD52 (A), CD84 (B), and PTGER2 (C) expression on reference mNDNs from HDs is reported only for the GD cohort because representative of reference mNDNs from HDs from all other cohorts. \*p < 0.05, \*\*p < 0.01, \*\*\*p < 0.001, \*\*\*\*p < 0.0001 by Kruskal-Wallis or Friedman test followed by Dunn’s multiple comparison test. See also Figures S5 and S6.

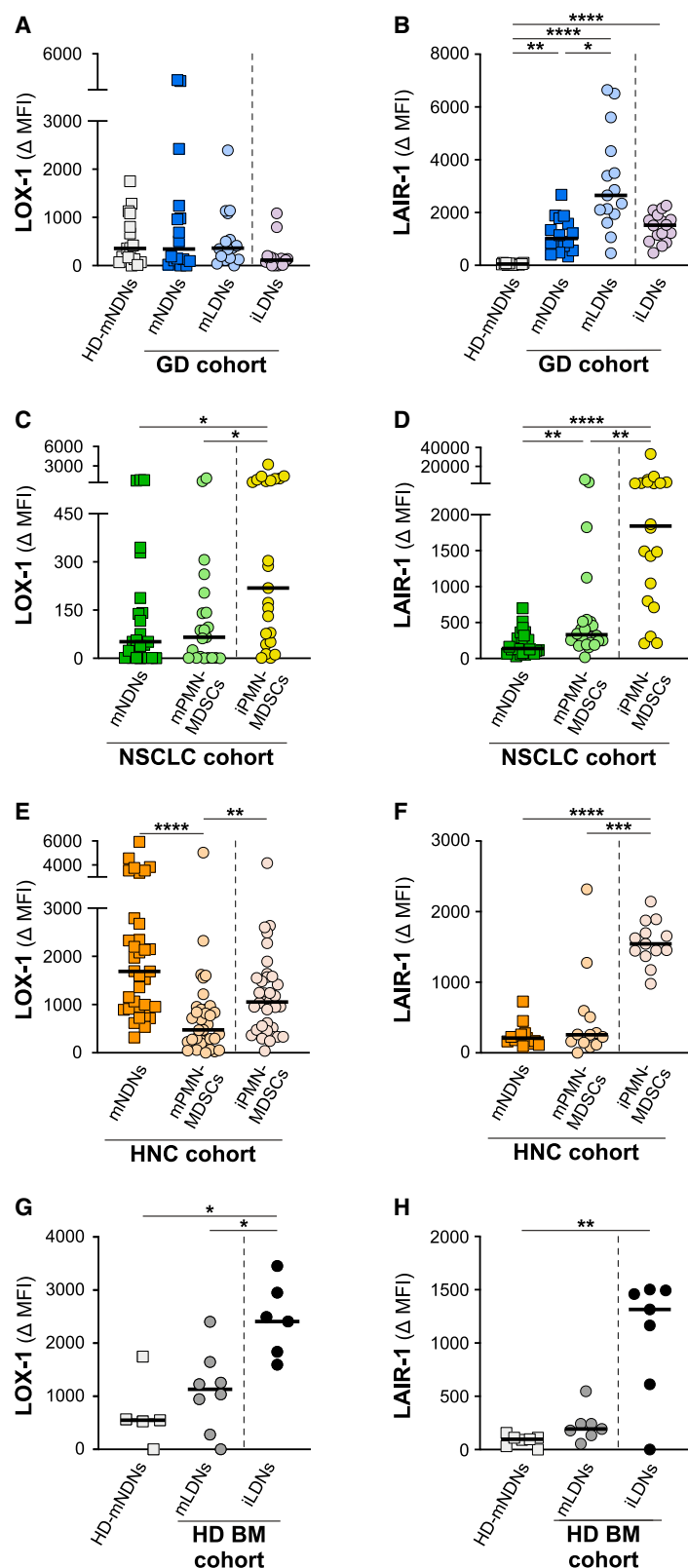


**Figure 7. Expression of surface LOX-1 and LAIR-1 on mPMN-MDSCs and iPMN-MDSC populations from GDs and cancer patients and on mature and immature LDNs from the BM of HDs**

Surface LOX-1 (A, C, E, and G) and LAIR-1 (B, D, F, and H) expression levels were evaluated by flow cytometry on mNDNs or mLDNs/iLDNs from GDs ( $n = 16-17$ ) and group-related mNDNs from HDs ( $n = 17$ ) (A and B), mPMN-MDSCs/iPMN-MDSCs and autologous mNDNs from cohorts of patients with NSCLC (C and D,  $n = 24-27$ ) and HNC (E and F,  $n = 13-35$ ), and mLDNs and iLDNs from BM aspirates from HDs ( $n = 6-8$ ) or control peripheral blood mNDNs from HDs (HD-mNDNs,  $n = 5-7$ ) (G and H). Graphs show LOX-1 or LAIR-1  $\Delta$  MFI values. Each symbol stands for a single donor sample. \* $p < 0.05$ , \*\* $p < 0.01$ , \*\*\* $p < 0.001$ , \*\*\*\* $p < 0.0001$  by Kruskal-Wallis or Friedman test followed by Dunn's multiple-comparisons test.



as the most consistently active TF regulons across all replicates of our mPMN-MDSC samples. While potential involvement of HBP1 in the regulation of PMN-MDSC generation/function has never been predicted, SMAD3 is known as a downstream TF of the TGF- $\beta$  superfamily,<sup>43</sup> of which TGF- $\beta$ 1 has been reported to be involved in the differentiation of both PMN-MDSCs<sup>17</sup> and pro tumor TANs<sup>44</sup> in mice. EGR1 was also very recently included among the specific TFs for lung cancer TANs.<sup>29</sup> Furthermore, consistent with the facts that hypoxia-linked stress has been reported to modulate MDSC development<sup>45,46</sup> and that an enrichment of genes belonging to the cell response to hypoxia pathways represent features of the mPMN-MDSC gene signature, it is noteworthy to highlight that EGR1 functions as a hypoxia-responsive TF.<sup>47</sup> Nevertheless, the potential role of the SMAD3 and EGR1 regulons in the modulation of human mPMN-MDSC generation, activation, and function should be experimentally validated.

The discovery of the mPMN-MDSC gene signature enabled us to identify potential PMN-MDSC-associated markers whose encoding genes were found to be included in a group of genes (7% of the total, named g2 genes) specifically upregulated in PMN-MDSC-committed neutrophils. Specifically, we observed that CD52, CD84, and PTGER2 are markedly upregulated on mNDNs/mLNs from GDs and mPMN-MDSCs from cancer patients compared with control mNDNs. CD52, CD84, and PTGER2 were also expressed on iPMN-MDSCs from cancer patients or iLDNs from GDs but at lower levels than on autologous mPMN-MDSCs (except for CD52 in NSCLC patients). However, none of these molecules were found to be expressed at detectable levels on immature neutrophils from HDs. It is therefore tempting to speculate that the enhanced expression of g2 genes/molecules, including CD52, CD84, and PTGER2, by mature compared with autologous immature PMN-MDSCs marks the acquisition of fully competent immunosuppressive functions by mPMN-MDSCs.<sup>12,14</sup>

It should be noted that, although CD84 has been proposed previously as a marker for PMN-MDSCs in breast cancer-bearing mice<sup>48</sup> or for total CD15<sup>+</sup>CD14<sup>−</sup>CD11b<sup>+</sup>HLA-DR<sup>−</sup>BM neutrophils from multiple myeloma patients,<sup>49</sup> CD84 expression on circulating mPMN-MDSCs has never been investigated, similar to that of PTGER2 and CD52. In any case, the biological roles previously proposed for CD52,<sup>50</sup> CD84,<sup>49</sup> and PTGER2<sup>51–54</sup> are consistent with our hypothesis and with our GO term enrichment analysis of g2 genes. On the other hand, even though g1 genes were found to encode proteins relevant for PMN-MDSC features (e.g., metabolic reprogramming, response to stress, etc.), the latter proteins are not appropriate as specific mPMN-MDSC-associated markers, as demonstrated here for LOX-1 and LAIR-1. With regard to LOX-1 (encoded by *OLR1*), which is often utilized as a PMN-MDSC marker,<sup>19,33–35</sup> we show that this molecule is constitutively expressed at high levels by immature BM neutrophils from HDs. This observation explains why, irrespective of their different immunoregulatory functions, total CD15<sup>+</sup>/CD66b<sup>+</sup> PMN-MDSCs of patients with various cancer types,<sup>19,33–35</sup> and even total CD15<sup>+</sup>/CD66b<sup>+</sup> LDNs of patients with SLE (which are proinflammatory and not immunosuppressive),<sup>10</sup> were found to display marked LOX-1 expression, likely determined by the immature neutrophil fraction included therein. Nevertheless, LOX-1-positive TANs<sup>29,55</sup> have been shown to display a mature phenotype and to

be associated with more potent MDSC activities than their LOX-1-negative tissue counterparts.<sup>55</sup>

Additionally, our findings further substantiate the notion that mNDNs/mLNs from GDs represent suitable cells to uncover the molecular and biological aspects of PMN-MDSCs,<sup>12</sup> which are often very rare in cancer patients and, consequently, difficult to isolate and study mechanistically. Why mPMN-MDSCs from GDs distribute between NDNs and LDNs remains, however, unclear.<sup>12</sup> We would speculate that the massive mobilization of both mature and immature neutrophils induced by the potent, G-CSF-dependent emergency granulopoiesis is followed by the differentiation of mLNs into mNDNs in the circulation after egress from the BM. In fact, despite their similar mature morphology,<sup>12</sup> gene expression analysis in this study revealed that mNDNs from GDs are at a more advanced maturation status than autologous mLNs. By contrast, mPMN-MDSCs of cancer patients are mobilized in lower numbers than mNDNs/mLNs from GDs and are not recovered within NDNs. It is, however, striking that the administration of G-CSF *in vivo* is sufficient to promote neutrophils to acquire molecular features shared by circulating PMN-MDSCs or even infiltrating TANs, as demonstrated in this study. Accordingly, G-CSF injection *in vivo* has been shown to induce overproduction of several cytokines/mediators<sup>56</sup> that are typically overabundant in the tumor microenvironment.<sup>57</sup> In this context, we also found that the mPMN-MDSC gene signature appears to be driven by a number of mediators, including GM-CSF, TGF- $\beta$ 1, IL-3, IL-6, IL-4, IL-13, and PTGS2, besides G-CSF. The functional, phenotypic, and transcriptomic similarities between mLNs/mNDNs from GDs and cancer mPMN-MDSCs are likely triggered, on one hand, by the common emergency granulopoiesis inducing their mobilization into the circulation and, on the other hand, by the consequent exposure to, besides G-CSF, multiple factors mimicking the cancer microenvironment. These observations may also explain why GDs, besides generating PMN-MDSCs (this study, Luyckx et al.,<sup>58</sup> and Vasconcelos et al.<sup>59</sup>), also display other typical cancer-associated features, such as an altered metabolomic profile<sup>60</sup> and/or the presence of other types of tolerogenic innate and adaptive immune cells.<sup>61</sup> In any case, it is also important to remark that G-CSF administration to HDs for stem cell mobilization<sup>62</sup> or as supportive treatment in chemotherapy-induced neutropenia in cancer patients<sup>63</sup> continues to have a favorable risk-benefit profile because most of the modulatory effects induced by the administration of this cytokine are thought to be transient and self-limiting.<sup>62,64</sup>

In summary, our data suggests that mPMN-MDSCs from cancer patients and GDs display distinct and similar transcriptional features associated with the acquisition of their immunosuppressive activities. Such common transcriptomes are acquired by neutrophils via gene reprogramming likely deriving from the combination of an altered maturation process (e.g., maintenance of g1 genes/block of g1 downregulation) together with an activation process caused by cell exposure to multiple exogenous/environmental mediators. Our results were obtained by both isolating pure populations of immunosuppressive versus non-immunosuppressive neutrophils at identical levels of maturation and focusing on genes/markers that are not expressed (or expressed at negligible levels) either on mature or on immature

normal neutrophils. This approach has never been undertaken before; for instance, in previous attempts aiming to define novel LDN/PMN-MDSC markers through either Cytometry by Time-Of-Flight (CyTOF)<sup>65</sup> or unbiased high-dimensional flow cytometry<sup>66</sup> or, as already mentioned, specific PMN-MDSC gene signatures.<sup>16,19,30,41</sup> The remarkable transcriptional and phenotypical differences between mPMN-MDSCs and *bona fide* neutrophils reported here demonstrate that the effort to distinguish mPMN-MDSCs only relying on a single, putative, surface marker is misleading.<sup>15,19,67–69</sup>

### Limitations of the study

Due to the limited numbers of subjects investigated, we could not evaluate the eventual influence of gender, race/ethnicity, and age in our experiments. We also did not address whether specific mPMN-MDSC subclusters express the distinct gene signature identified here by bulk RNA-seq experiments or whether subpopulations of mPMN-MDSCs co-expressing CD52, CD84, and PTGER2 exist in cancer patients. Finally, although this work does not exclude that additional mPMN-MDSC markers may exist, an evaluation of the immunosuppressive capacity eventually exerted by any possible CD52<sup>+</sup>, CD84<sup>+</sup>, and/or PTGER2<sup>+</sup> mPMN-MDSC subpopulations is required or necessary.

### STAR★METHODS

Detailed methods are provided in the online version of this paper and include the following:

- **KEY RESOURCES TABLE**
- **RESOURCE AVAILABILITY**
  - Lead contact
  - Materials availability
  - Data and code availability
- **EXPERIMENTAL MODEL AND STUDY PARTICIPANT DETAILS**
  - Study participants
  - Cell lines and primary cells
- **METHOD DETAILS**
  - Cell isolation and culture
  - Flow cytometry experiments
  - T cell proliferation assay
  - Cell cytotoxicity assay
  - RT-qPCR
  - RNA sequencing (RNA-seq)
  - RNA-seq library preparation
  - RNA-seq computational analysis
  - K-means clustering and cluster overlap analysis
  - Analysis of TF regulons and upstream regulators
  - Enrichment of the gene signature in bulk RNA-seq data
  - GO enrichment analysis
  - Gene signature expression in neutrophil precursors
  - Single-cell RNA-seq (scRNA-seq)
  - Seven Bridges processing for scRNA-seq data
  - Seurat workflow for scRNA-seq data analysis
  - Seurat workflow for published scRNA-seq datasets
- **QUANTIFICATION AND STATISTICAL ANALYSIS**

### SUPPLEMENTAL INFORMATION

Supplemental information can be found online at <https://doi.org/10.1016/j.xcrm.2023.101380>.

### ACKNOWLEDGMENTS

This work was supported by grants from Associazione Italiana per la Ricerca sul Cancro (AIRC; IG20339 and IG27613) and Fondazione Cariverona (8974/2017) (to M.A.C.); Ministero dell'Istruzione, dell'Università e della Ricerca (MIUR-PRIN20227YR8AW to M.A.C. and MIUR-PRIN20174T7NXL to F.B.), Università di Verona (RBVR17NCNC) (to P.S.), Ministry of Health (Italy) grant GR-2016-02361263 (to N.T.), and the German Research Foundation (DFG) through Collaborative Research Center (TRR) 332 (project A4 to S.B.). This work was also supported by European Cooperation in Science and Technology (COST) Actions BM1404 Mye-EUNITER (<https://www.cost.eu/actions/BM1404/>) and CA20117 Mye-InfoBank ([www.mye-infobank.eu](http://www.mye-infobank.eu)); COST is supported by the EU Framework Program Horizon 2020. We thank CPT of Verona University, which has been instrumental for access to flow cytometry/cell analysis and the genomic/transcriptomic and the computational platforms. We thank Stefano Ugel and Vincenzo Bronte (University of Verona) for help with cancer patient recruitment.

### AUTHOR CONTRIBUTIONS

F.P., K.B., M.D., S.C., O.M., G.I., E.C., F.C., and M.G. performed and analyzed flow cytometry, cell sorting, and *in vitro* functional experiments. S.G., E.G., and M.C. prepared cellular samples for RNA-seq. B.M. analyzed RNA-seq data. C.L. analyzed scRNA-seq data. F.B.-A. and N.T. supervised and contributed to RNA-seq and scRNA-seq data analysis. M.C., A.V., and D.P. provided GD blood samples and collected data. M.M., A.V., and D.P. provided NSCLC and BC patient blood samples and collected data. B. Höing, M.C.S., and T.H. provided HNC patient samples and collected data. B. Hadaschik and C.K. provided RCC and TCC patient samples and collected data. C.T. and C.V. provided DLBCL patient blood samples and collected data. L.K. provided LPS-treated donor samples. F.B., L.K., and S.D. contributed to the final approval of the manuscript version to be submitted. F.P., B.M., C.L., N.T., S.B., M.A.C., and P.S. designed and wrote the manuscript. S.B. supervised parts of the study. M.A.C. and P.S. conceptualized the study and supervised parts of the study.

### DECLARATION OF INTERESTS

The authors declare no competing interests.

Received: March 7, 2023

Revised: August 11, 2023

Accepted: December 18, 2023

Published: January 18, 2024

### REFERENCES

1. Hacbarth, E., and Kajdacsy-Balla, A. (1986). Low density neutrophils in patients with systemic lupus erythematosus, rheumatoid arthritis, and acute rheumatic fever. *Arthritis Rheum.* 29, 1334–1342.
2. Scapini, P., Marini, O., Tecchio, C., and Cassatella, M.A. (2016). Human neutrophils in the saga of cellular heterogeneity: insights and open questions. *Immunol. Rev.* 273, 48–60.
3. Silvestre-Roig, C., Fridlender, Z.G., Glogauer, M., and Scapini, P. (2019). Neutrophil Diversity in Health and Disease. *Trends Immunol.* 40, 565–583.
4. Denny, M.F., Yalavarthi, S., Zhao, W., Thacker, S.G., Anderson, M., Sandy, A.R., McCune, W.J., and Kaplan, M.J. (2010). A distinct subset of proinflammatory neutrophils isolated from patients with systemic lupus erythematosus induces vascular damage and synthesizes type I IFNs. *J. Immunol.* 184, 3284–3297.

5. Ochoa, A.C., Zea, A.H., Hernandez, C., and Rodríguez, P.C. (2007). Arginase, prostaglandins, and myeloid-derived suppressor cells in renal cell carcinoma. *Clin. Cancer Res.* **13**, 721s–726s.
6. Veglia, F., Sanseviero, E., and Gabrilovich, D.I. (2021). Myeloid-derived suppressor cells in the era of increasing myeloid cell diversity. *Nat. Rev. Immunol.* **21**, 485–498.
7. Zea, A.H., Rodríguez, P.C., Atkins, M.B., Hernandez, C., Signoretti, S., Zabaleta, J., McDermott, D., Quiceno, D., Youmans, A., O'Neill, A., et al. (2005). Arginase-producing myeloid suppressor cells in renal cell carcinoma patients: a mechanism of tumor evasion. *Cancer Res.* **65**, 3044–3048.
8. Cassetta, L., Bruderek, K., Skrzeczynska-Moncznik, J., Osiecka, O., Hu, X., Rundgren, I.M., Lin, A., Santegoets, K., Horzum, U., Godinho-Santos, A., et al. (2020). Differential expansion of circulating human MDSC subsets in patients with cancer, infection and inflammation. *J. Immunother. Cancer* **8**, e001223.
9. Mistry, P., Nakabo, S., O'Neil, L., Goel, R.R., Jiang, K., Carmona-Rivera, C., Gupta, S., Chan, D.W., Carlucci, P.M., Wang, X., et al. (2019). Transcriptomic, epigenetic, and functional analyses implicate neutrophil diversity in the pathogenesis of systemic lupus erythematosus. *Proc. Natl. Acad. Sci. USA* **116**, 25222–25228.
10. Rahman, S., Sagar, D., Hanna, R.N., Lightfoot, Y.L., Mistry, P., Smith, C.K., Manna, Z., Hasni, S., Siegel, R.M., Sanjuan, M.A., et al. (2019). Low-density granulocytes activate T cells and demonstrate a non-suppressive role in systemic lupus erythematosus. *Ann. Rheum. Dis.* **78**, 957–966.
11. Brandau, S., Trellakis, S., Bruderek, K., Schmaltz, D., Steller, G., Elian, M., Suttman, H., Schenck, M., Welling, J., Zabel, P., and Lang, S. (2011). Myeloid-derived suppressor cells in the peripheral blood of cancer patients contain a subset of immature neutrophils with impaired migratory properties. *J. Leukoc. Biol.* **89**, 311–317.
12. Marini, O., Costa, S., Bevilacqua, D., Calzetti, F., Tamassia, N., Spina, C., De Sabata, D., Tinazzi, E., Lunardi, C., Scupoli, M.T., et al. (2017). Mature CD10(+) and immature CD10(-) neutrophils present in G-CSF-treated donors display opposite effects on T cells. *Blood* **129**, 1343–1356.
13. Gabrilovich, D.I., and Nagaraj, S. (2009). Myeloid-derived suppressor cells as regulators of the immune system. *Nat. Rev. Immunol.* **9**, 162–174.
14. Lang, S., Bruderek, K., Kaspar, C., Höing, B., Kanaan, O., Dominas, N., Hussain, T., Droge, F., Eyth, C., Hadaschik, B., and Brandau, S. (2018). Clinical Relevance and Suppressive Capacity of Human Myeloid-Derived Suppressor Cell Subsets. *Clin. Cancer Res.* **24**, 4834–4844.
15. Perez, C., Botta, C., Zabaleta, A., Puig, N., Cedena, M.T., Goicoechea, I., Alameda, D., San José-Eneriz, E., Merino, J., Rodríguez-Otero, P., et al. (2020). Immunogenomic identification and characterization of granulocytic myeloid-derived suppressor cells in multiple myeloma. *Blood* **136**, 199–209.
16. Pelosi, A., Besi, F., Tumino, N., Merli, P., Quatrini, L., Li Pira, G., Algeri, M., Moretta, L., and Vacca, P. (2021). NK Cells and PMN-MDSCs in the Graft From G-CSF Mobilized Haploidentical Donors Display Distinct Gene Expression Profiles From Those of the Non-Mobilized Counterpart. *Front. Immunol.* **12**, 657329.
17. Sagiv, J.Y., Michaeli, J., Assi, S., Mishalian, I., Kisos, H., Levy, L., Damti, P., Lumbroso, D., Polyansky, L., Sionov, R.V., et al. (2015). Phenotypic diversity and plasticity in circulating neutrophil subpopulations in cancer. *Cell Rep.* **10**, 562–573.
18. Köstlin, N., Ostermeier, A.L., Spring, B., Schwarz, J., Marmé, A., Walter, C.B., Poets, C.F., and Gille, C. (2017). HLA-G promotes myeloid-derived suppressor cell accumulation and suppressive activity during human pregnancy through engagement of the receptor ILT4. *Eur. J. Immunol.* **47**, 374–384.
19. Condomine, T., Dominguez, G.A., Youn, J.I., Kossenkova, A.V., Mony, S., Alicea-Torres, K., Tcyganov, E., Hashimoto, A., Nefedova, Y., Lin, C., et al. (2016). Lectin-type oxidized LDL receptor-1 distinguishes population of human polymorphonuclear myeloid-derived suppressor cells in cancer patients. *Sci. Immunol.* **1**, aaf8943.
20. Sangaletti, S., Talarico, G., Chiodoni, C., Cappetti, B., Botti, L., Portararo, P., Gulino, A., Consonni, F.M., Sica, A., Randon, G., et al. (2019). SPARC Is a New Myeloid-Derived Suppressor Cell Marker Licensing Suppressive Activities. *Front. Immunol.* **10**, 1369.
21. Garcia-Alonso, L., Holland, C.H., Ibrahim, M.M., Turei, D., and Saez-Rodriguez, J. (2019). Benchmark and integration of resources for the estimation of human transcription factor activities. *Genome Res.* **29**, 1363–1375.
22. Alvarez, M.J., Shen, Y., Giorgi, F.M., Lachmann, A., Ding, B.B., Ye, B.H., and Califano, A. (2016). Functional characterization of somatic mutations in cancer using network-based inference of protein activity. *Nat. Genet.* **48**, 838–847.
23. Aarts, C.E.M., Hiemstra, I.H., Béguin, E.P., Hoogendijk, A.J., Bouchmal, S., van Houdt, M., Tool, A.T.J., Mul, E., Jansen, M.H., Janssen, H., et al. (2019). Activated neutrophils exert myeloid-derived suppressor cell activity damaging T cells beyond repair. *Blood Adv.* **3**, 3562–3574.
24. Maneta, E., Fultang, L., Taylor, J., Pugh, M., Jenkinson, W., Anderson, G., Coomarasamy, A., Kilby, M.D., Lissauer, D.M., Mussai, F., and De Santo, C. (2022). G-CSF induces CD15(+) CD14(+) cells from granulocytes early in the physiological environment of pregnancy and the cancer immunosuppressive microenvironment. *Clin. Transl. Immunology* **11**, e1395.
25. Millrud, C.R., Bergenfelz, C., and Leanderson, K. (2017). On the origin of myeloid-derived suppressor cells. *Oncotarget* **8**, 3649–3665.
26. Rotondo, R., Bertolotto, M., Barisione, G., Astigiano, S., Mandruzzato, S., Ottonello, L., Dallegri, F., Bronte, V., Ferrini, S., and Barbieri, O. (2011). Exocytosis of azurophil and arginase 1-containing granules by activated polymorphonuclear neutrophils is required to inhibit T lymphocyte proliferation. *J. Leukoc. Biol.* **89**, 721–727.
27. Schmielau, J., and Finn, O.J. (2001). Activated granulocytes and granulocyte-derived hydrogen peroxide are the underlying mechanism of suppression of t-cell function in advanced cancer patients. *Cancer Res.* **61**, 4756–4760.
28. Pillay, J., Kamp, V.M., van Hoffen, E., Visser, T., Tak, T., Lammers, J.W., Ulfman, L.H., Leenen, L.P., Pickkers, P., and Koenderman, L. (2012). A subset of neutrophils in human systemic inflammation inhibits T cell responses through Mac-1. *J. Clin. Invest.* **122**, 327–336.
29. Salcher, S., Sturm, G., Horvath, L., Untergasser, G., Kuempers, C., Fotakis, G., Panizzolo, E., Martowicz, A., Trebo, M., Pall, G., et al. (2022). High-resolution single-cell atlas reveals diversity and plasticity of tissue-resident neutrophils in non-small cell lung cancer. *Cancer Cell* **40**, 1503–1520.e8.
30. Zilionis, R., Engblom, C., Pfirschke, C., Savova, V., Zemmour, D., Saaticoglu, H.D., Krishnan, I., Maroni, G., Meyerovitz, C.V., Kerwin, C.M., et al. (2019). Single-Cell Transcriptomics of Human and Mouse Lung Cancers Reveals Conserved Myeloid Populations across Individuals and Species. *Immunity* **50**, 1317–1334.e10.
31. Grassi, L., Pourfarzad, F., Ullrich, S., Merkel, A., Were, F., Carrillo-de-Santa-Pau, E., Yi, G., Hiemstra, I.H., Tool, A.T.J., Mul, E., et al. (2018). Dynamics of Transcription Regulation in Human Bone Marrow Myeloid Differentiation to Mature Blood Neutrophils. *Cell Rep.* **24**, 2784–2794.
32. Calzetti, F., Finotti, G., Tamassia, N., Bianchetto-Aguilera, F., Castellucci, M., Canè, S., Lonardi, S., Cavallini, C., Matte, A., Gasperini, S., et al. (2022). CD66b(-)CD64(dim)CD115(-) cells in the human bone marrow represent neutrophil-committed progenitors. *Nat. Immunol.* **23**, 679–691.
33. Chai, E., Zhang, L., and Li, C. (2019). LOX-1+ PMN-MDSC enhances immune suppression which promotes glioblastoma multiforme progression. *Cancer Manag. Res.* **11**, 7307–7315.
34. Nan, J., Xing, Y.F., Hu, B., Tang, J.X., Dong, H.M., He, Y.M., Ruan, D.Y., Ye, Q.J., Cai, J.R., Ma, X.K., et al. (2018). Endoplasmic reticulum stress induced LOX-1(+) CD15(+) polymorphonuclear myeloid-derived suppressor cells in hepatocellular carcinoma. *Immunology* **154**, 144–155.

35. Kim, H.R., Park, S.M., Seo, S.U., Jung, I., Yoon, H.I., Gabrilovich, D.I., Cho, B.C., Seong, S.Y., Ha, S.J., and Youn, J.I. (2019). The Ratio of Peripheral Regulatory T Cells to Lox-1(+) Polymorphonuclear Myeloid-derived Suppressor Cells Predicts the Early Response to Anti-PD-1 Therapy in Patients with Non-Small Cell Lung Cancer. *Am. J. Respir. Crit. Care Med.* **199**, 243–246.
36. Xu, L., Wang, S., Li, J., Li, J., and Li, B. (2020). Cancer immunotherapy based on blocking immune suppression mediated by an immune modulator LAIR-1. *Oncolimmunology* **9**, 1740477.
37. Brandau, S., Moses, K., and Lang, S. (2013). The kinship of neutrophils and granulocytic myeloid-derived suppressor cells in cancer: cousins, siblings or twins? *Semin. Cancer Biol.* **23**, 171–182.
38. Bronte, V., Brandau, S., Chen, S.H., Colombo, M.P., Frey, A.B., Greten, T.F., Mandruzzato, S., Murray, P.J., Ochoa, A., Ostrand-Rosenberg, S., et al. (2016). Recommendations for myeloid-derived suppressor cell nomenclature and characterization standards. *Nat. Commun.* **7**, 12150.
39. Pillay, J., Tak, T., Kamp, V.M., and Koenderman, L. (2013). Immune suppression by neutrophils and granulocytic myeloid-derived suppressor cells: similarities and differences. *Cell. Mol. Life Sci.* **70**, 3813–3827.
40. Quail, D.F., Amulic, B., Aziz, M., Barnes, B.J., Eruslanov, E., Fridlender, Z.G., Goodridge, H.S., Granot, Z., Hidalgo, A., Huttenlocher, A., et al. (2022). Neutrophil phenotypes and functions in cancer: A consensus statement. *J. Exp. Med.* **219**, e20220011.
41. Veglia, F., Hashimoto, A., Dweep, H., Sanseviero, E., De Leo, A., Tcyganov, E., Kossenkova, A., Mulligan, C., Nam, B., Masters, G., et al. (2021). Analysis of classical neutrophils and polymorphonuclear myeloid-derived suppressor cells in cancer patients and tumor-bearing mice. *J. Exp. Med.* **218**, e20201803.
42. Xue, R., Zhang, Q., Cao, Q., Kong, R., Xiang, X., Liu, H., Feng, M., Wang, F., Cheng, J., Li, Z., et al. (2022). Liver tumour immune microenvironment subtypes and neutrophil heterogeneity. *Nature* **612**, 141–147.
43. Schmierer, B., and Hill, C.S. (2007). TGFβ-SMAD signal transduction: molecular specificity and functional flexibility. *Nat. Rev. Mol. Cell Biol.* **8**, 970–982.
44. Fridlender, Z.G., Sun, J., Kim, S., Kapoor, V., Cheng, G., Ling, L., Worthen, G.S., and Albelda, S.M. (2009). Polarization of tumor-associated neutrophil phenotype by TGF-β: "N1" versus "N2" TAN. *Cancer Cell* **16**, 183–194.
45. Corzo, C.A., Condamine, T., Lu, L., Cotter, M.J., Youn, J.I., Cheng, P., Cho, H.I., Celis, E., Quiceno, D.G., Padhya, T., et al. (2010). HIF-1α regulates function and differentiation of myeloid-derived suppressor cells in the tumor microenvironment. *J. Exp. Med.* **207**, 2439–2453.
46. Mandula, J.K., and Rodriguez, P.C. (2021). Tumor-related stress regulates functional plasticity of MDSCs. *Cell. Immunol.* **363**, 104312.
47. Elbarghati, L., Murdoch, C., and Lewis, C.E. (2008). Effects of hypoxia on transcription factor expression in human monocytes and macrophages. *Immunobiology* **213**, 899–908.
48. Alshetaiwi, H., Pervolarakis, N., McIntyre, L.L., Ma, D., Nguyen, Q., Rath, J.A., Nee, K., Hernandez, G., Evans, K., Torosian, L., et al. (2020). Defining the emergence of myeloid-derived suppressor cells in breast cancer using single-cell transcriptomics. *Sci. Immunol.* **5**, eaay6017.
49. Lewinsky, H., Gunes, E.G., David, K., Radomir, L., Kramer, M.P., Pellegrino, B., Perpinial, M., Chen, J., He, T.F., Mansour, A.G., et al. (2021). CD84 is a regulator of the immunosuppressive microenvironment in Multiple Myeloma. *JCI Insight* **6**, e141683.
50. Bandala-Sanchez, E., G Bediaga, N., Goddard-Borger, E.D., Ngui, K., Naselli, G., Stone, N.L., Neale, A.M., Pearce, L.A., Wardak, A., Czabotar, P., et al. (2018). CD52 glycan binds the proinflammatory B box of HMGB1 to engage the Siglec-10 receptor and suppress human T cell function. *Proc. Natl. Acad. Sci. USA* **115**, 7783–7788.
51. Obermajer, N., Muthuswamy, R., Odunsi, K., Edwards, R.P., and Kalinski, P. (2011). PGE(2)-induced CXCL12 production and CXCR4 expression controls the accumulation of human MDSCs in ovarian cancer environment. *Cancer Res.* **71**, 7463–7470.
52. Porta, C., Consonni, F.M., Morlacchi, S., Sangaletti, S., Bleve, A., Totaro, M.G., Larghi, P., Rimoldi, M., Tripodo, C., Strauss, L., et al. (2020). Tumor-Derived Prostaglandin E2 Promotes p50 NF-κB-Dependent Differentiation of Monocytic MDSCs. *Cancer Res.* **80**, 2874–2888.
53. Rodríguez-Ubrea, J., Català-Moll, F., Obermajer, N., Álvarez-Erriro, D., Ramirez, R.N., Company, C., Vento-Tormo, R., Moreno-Bueno, G., Edwards, R.P., Mortazavi, A., et al. (2017). Prostaglandin E2 Leads to the Acquisition of DNMT3A-Dependent Tolerogenic Functions in Human Myeloid-Derived Suppressor Cells. *Cell Rep.* **21**, 154–167.
54. Sinha, P., Clements, V.K., Fulton, A.M., and Ostrand-Rosenberg, S. (2007). Prostaglandin E2 promotes tumor progression by inducing myeloid-derived suppressor cells. *Cancer Res.* **67**, 4507–4513.
55. Si, Y., Merz, S.F., Jansen, P., Wang, B., Bruderek, K., Altenhoff, P., Mattheis, S., Lang, S., Gunzer, M., Klode, J., et al. (2019). Multidimensional imaging provides evidence for down-regulation of T cell effector function by MDSC in human cancer tissue. *Sci. Immunol.* **4**, eaaw9159.
56. Xu, S., Höglund, M., Håkansson, L., and Venge, P. (2000). Granulocyte colony-stimulating factor (G-CSF) induces the production of cytokines in vivo. *Br. J. Haematol.* **108**, 848–853.
57. Burkholder, B., Huang, R.Y., Burgess, R., Luo, S., Jones, V.S., Zhang, W., Lv, Z.Q., Gao, C.Y., Wang, B.L., Zhang, Y.M., and Huang, R.P. (2014). Tumor-induced perturbations of cytokines and immune cell networks. *Biochim. Biophys. Acta* **1845**, 182–201.
58. Luyckx, A., Schouppe, E., Rutgeerts, O., Lenaerts, C., Fevery, S., Devos, T., Dierckx, D., Waer, M., Van Ginderachter, J.A., and Billiau, A.D. (2012). G-CSF stem cell mobilization in human donors induces polymorphonuclear and mononuclear myeloid-derived suppressor cells. *Clin. Immunol.* **143**, 83–87.
59. Vasconcelos, Z.F.M., Santos, B.M., Costa, E.S., Lima, M., Tabak, D.G., Bouzas, L.F., Azevedo, W.M., Barcinski, M.A., and Bonomo, A. (2003). T-lymphocyte function from peripheral blood stem-cell donors is inhibited by activated granulocytes. *Cytotherapy* **5**, 336–345.
60. Hatfield, K.J., Melve, G.K., and Bruserud, Ø. (2017). Granulocyte colony-stimulating factor alters the systemic metabolomic profile in healthy donors. *Metabolomics* **13**, 2.
61. Yang, J.Z., Zhang, J.Q., and Sun, L.X. (2016). Mechanisms for T cell tolerance induced with granulocyte colony-stimulating factor. *Mol. Immunol.* **70**, 56–62.
62. Anderlini, P. (2009). Effects and safety of granulocyte colony-stimulating factor in healthy volunteers. *Curr. Opin. Hematol.* **16**, 35–40.
63. Yeo, B., Redfern, A.D., Mouchemore, K.A., Hamilton, J.A., and Anderson, R.L. (2018). The dark side of granulocyte-colony stimulating factor: a supportive therapy with potential to promote tumour progression. *Clin. Exp. Metastasis* **35**, 255–267.
64. Mouchemore, K.A., and Anderson, R.L. (2021). Immunomodulatory effects of G-CSF in cancer: Therapeutic implications. *Semin. Immunol.* **54**, 101512.
65. Shaul, M.E., Eyal, O., Guglietta, S., Aloni, P., Zlotnik, A., Forkosh, E., Levy, L., Weber, L.M., Levin, Y., Pomerantz, A., et al. (2020). Circulating neutrophil subsets in advanced lung cancer patients exhibit unique immune signature and relate to prognosis. *FASEB J* **34**, 4204–4218.
66. Valadez-Cosmes, P., Maitz, K., Kindler, O., Raftopoulou, S., Kienzl, M., Santiso, A., Mihalic, Z.N., Brcic, L., Lindenmann, J., Fediuk, M., et al. (2021). Identification of Novel Low-Density Neutrophil Markers Through Unbiased High-Dimensional Flow Cytometry Screening in Non-Small Cell Lung Cancer Patients. *Front. Immunol.* **12**, 703846.
67. Al-Khami, A.A., Zheng, L., Del Valle, L., Hossain, F., Wyczzechowska, D., Zabaleta, J., Sanchez, M.D., Dean, M.J., Rodriguez, P.C., and Ochoa, A.C. (2017). Exogenous lipid uptake induces metabolic and functional reprogramming of tumor-associated myeloid-derived suppressor cells. *Oncolimmunology* **6**, e1344804.



68. Karakasheva, T.A., Dominguez, G.A., Hashimoto, A., Lin, E.W., Chiu, C., Sasser, K., Lee, J.W., Beatty, G.L., Gabrilovich, D.I., and Rustgi, A.K. (2018). CD38+ M-MDSC expansion characterizes a subset of advanced colorectal cancer patients. *JCI Insight* 3, e97022.
69. Zhang, J., Xu, X., Shi, M., Chen, Y., Yu, D., Zhao, C., Gu, Y., Yang, B., Guo, S., Ding, G., et al. (2017). CD13(hi) Neutrophil-like myeloid-derived suppressor cells exert immune suppression through Arginase 1 expression in pancreatic ductal adenocarcinoma. *Oncolimmunology* 6, e1258504.
70. Tamassia, N., Bianchetto-Aguilera, F., Gasperini, S., Polletti, S., Gardiman, E., Ostuni, R., Natoli, G., and Cassatella, M.A. (2021). Induction of OCT2 contributes to regulate the gene expression program in human neutrophils activated via TLR8. *Cell Rep.* 35, 109143.
71. Picelli, S., Björklund, A.K., Reinius, B., Sagasser, S., Winberg, G., and Sandberg, R. (2014). Tn5 transposase and tagmentation procedures for massively scaled sequencing projects. *Genome Res.* 24, 2033–2040.
72. Kim, D., Paggi, J.M., Park, C., Bennett, C., and Salzberg, S.L. (2019). Graph-based genome alignment and genotyping with HISAT2 and HISAT-genotype. *Nat. Biotechnol.* 37, 907–915.
73. Anders, S., Pyl, P.T., and Huber, W. (2015). HTSeq—a Python framework to work with high-throughput sequencing data. *Bioinformatics* 31, 166–169.
74. Love, M.I., Huber, W., and Anders, S. (2014). Moderated estimation of fold change and dispersion for RNA-seq data with DESeq2. *Genome Biol.* 15, 550.
75. Risso, D., Ngai, J., Speed, T.P., and Dudoit, S. (2014). Normalization of RNA-seq data using factor analysis of control genes or samples. *Nat. Biotechnol.* 32, 896–902.
76. Mi, H., Muruganujan, A., and Thomas, P.D. (2013). PANTHER in 2013: modeling the evolution of gene function, and other gene attributes, in the context of phylogenetic trees. *Nucleic Acids Res.* 41, D377–D386.
77. Supek, F., Bošnjak, M., Škunca, N., and Šmuc, T. (2011). REVIGO summarizes and visualizes long lists of gene ontology terms. *PLoS One* 6, e21800.
78. Krämer, A., Green, J., Pollard, J., Jr., and Tugendreich, S. (2014). Causal analysis approaches in Ingenuity Pathway Analysis. *Bioinformatics* 30, 523–530.
79. Hao, Y., Hao, S., Andersen-Nissen, E., Mauck, W.M., 3rd, Zheng, S., Butler, A., Lee, M.J., Wilk, A.J., Darby, C., Zager, M., et al. (2021). Integrated analysis of multimodal single-cell data. *Cell* 184, 3573–3587.e29.
80. Korsunsky, I., Millard, N., Fan, J., Slowikowski, K., Zhang, F., Wei, K., Baglaenko, Y., Brenner, M., Loh, P.R., and Raychaudhuri, S. (2019). Fast, sensitive and accurate integration of single-cell data with Harmony. *Nat. Methods* 16, 1289–1296.
81. Andreatta, M., and Carmona, S.J. (2021). UCell: Robust and scalable single-cell gene signature scoring. *Comput. Struct. Biotechnol. J.* 19, 3796–3798.
82. Leek, J.T., Johnson, W.E., Parker, H.S., Jaffe, A.E., and Storey, J.D. (2012). The sva package for removing batch effects and other unwanted variation in high-throughput experiments. *Bioinformatics* 28, 882–883.
83. Bruger, A.M., Vanhaver, C., Bruderek, K., Amodio, G., Tavukçuoğlu, E., Esendagli, G., Gregori, S., Brandau, S., and van der Bruggen, P. (2020). Protocol to assess the suppression of T-cell proliferation by human MDSC. *Methods Enzymol.* 632, 155–192.
84. Gong, Z., Li, Q., Shi, J., Li, P., Hua, L., Shultz, L.D., and Ren, G. (2023). Immunosuppressive reprogramming of neutrophils by lung mesenchymal cells promotes breast cancer metastasis. *Sci. Immunol.* 8, eadd5204.
85. Thomas, P.D., Campbell, M.J., Kejariwal, A., Mi, H., Karlak, B., Daverman, R., Diemer, K., Muruganujan, A., and Narechania, A. (2003). PANTHER: a library of protein families and subfamilies indexed by function. *Genome Res.* 13, 2129–2141.



## STAR★METHODS

## KEY RESOURCES TABLE

REAGENT or RESOURCE	SOURCE	IDENTIFIER
<b>Antibodies</b>		
anti-human CD56-PE (clone REA196) – Lab 1	Miltenyi Biotec	Cat# 130-112-312; RRID: AB_2726090
anti-human CD45-BV510 (clone HI30) – Lab 1	BioLegend	Cat# 304036; RRID: AB_2561940
anti-human CD45-VioGreen (clone 5B1) – Lab 2	Miltenyi Biotec	Cat# 130-113-124; RRID: AB_2725952
anti-human CD66b-FITC (clone G10F5) – Lab 1	BioLegend	Cat# 305104; RRID: AB_314496
anti-human CD66b-APC (clone G10F5) – Lab 1	BioLegend	Cat# 305118; RRID: AB_2566607
anti-human CD66b-PerCP-Cy5.5 (clone G10F5) – Lab 2	BioLegend	Cat# 305108; RRID: AB_2077855
anti-human CD66b-BV421 (clone 6/40c) – Lab 2	BioLegend	Cat# 392916; RRID: AB_2888722
anti-human CD11b-PE-Cy7 (clone ICRF44) – Lab 1	BioLegend	Cat# 301322; RRID: AB_830644
anti-human CD11b-APC-Cy7 (clone ICRF44) – Lab 1	BioLegend	Cat#301342; RRID: AB_2563395
anti-human CD11b-APC-Cy7 (clone ICRF44) – Lab 2	BD Biosciences	Cat# 557754; RRID: AB_396860
anti-human CD16-APC-Cy7 (clone 3G8) – Lab 1	BioLegend	Cat# 301018; RRID: AB_314218
anti-human CD16-PE-Cy7 (clone 3G8) – Lab 2	BD Biosciences	Cat# 557744; RRID: AB_396850
anti-human CD16-PerCP-Cy5.5 (clone 3G8) – Lab 1	BioLegend	Cat# 302028; RRID: AB_893263
anti-human CD10-PE (clone HI10a) – Lab 1	BioLegend	Cat# 312204; RRID: AB_314915
anti-human CD10-PE-Vio 770 (clone REA877) – Lab 1	Miltenyi Biotec	Cat# 130-114-504; RRID: AB_2726674
anti-human CD10-APC (clone HI10a) – Lab 2	BioLegend	Cat# 312210; RRID: AB_314921
anti-human CD10-BV650 (clone HI10a) – Lab 1	BD Biosciences	Cat# 563734; RRID: AB_2738393
anti-human CD62L-APC (clone 145/15) – Lab 1	Miltenyi Biotec	Cat# 130-113-617; RRID: AB_2733392
anti-human CD84-FITC (clone REA1102) – Lab 1	Miltenyi Biotec	Cat# 130-119-034; RRID: AB_2751611
anti-human CD84-PE (clone REA1102) – Lab 2	Miltenyi Biotec	Cat# 130-119-035; RRID: AB_2751612
anti-human CD84-PE (clone CD84.1.21) – Lab 1	BioLegend	Cat# 326008; RRID: AB_2229003
anti-human PTGER2-FITC (polyclonal) – Lab 1/2	biortbyt	Cat# orb7558; RRID: AB_10938289
anti-human PTGER2-AF488 (clone EPR8030) – Lab 1/2	abcam	Cat# ab246777
anti-human CD52-FITC (clone HI186) – Lab 1/2	BioLegend	Cat# 316004; RRID: AB_389277
anti-human CD52-Alexa Fluor 405 (clone HI186) – Lab 1	Novus Biologicals	Cat# NB500-311AF405
anti-human CD52-PerCP-Cy5.5 (clone HI186) – Lab 2	BioLegend	Cat# 316010; RRID: AB_2650807
anti-human LOX-1-APC (clone 15C4) – Lab 1	BioLegend	Cat# 358606; RRID: AB_2563473
anti-human LOX-1-PE (clone 15C4) – Lab 2	BioLegend	Cat# 358604; RRID: AB_2562181
anti-human LAIR-1-VioBright-FITC (clone REA447) – Lab 1	Miltenyi Biotec	Cat# 130-106-852; RRID: AB_2657221
anti-human LAIR-1-PE (clone REA447) – Lab 2	Miltenyi Biotec	Cat# 130-106-849; RRID: AB_2657223
Human CD3 epsilon (clone UCHT1)	R&D Systems	Cat# MAB100-500; RRID: AB_357359
anti-human CD28 (clone CD28.2)	BioLegend	Cat# 302934; RRID: AB_11148949
<b>Experimental models: Cell lines</b>		
Human: K562 cells	ATCC	CCL-243
<b>Chemicals, peptides, and recombinant proteins</b>		
PrimeScript™ RT Reagent (Perfect Real-Time)	Takara	Cat# RR037A
TB green® premix Ex Taq™ (Tli RNaseH Plus)	Takara	Cat# RR420W
KAPA HiFi HotStart PCR kit	KAPABIOSYSTEMS	Cat# KK2502
Cell Proliferation ELISA, BrdU (colorimetric)	Roche	Cat# 11647229001
CellTrace™ CFSE Cell Proliferation kit	ThermoFisher Scientific	Cat# C34570
CellTracker™ GREEN CMFDA Dye	Invitrogen	Cat# C2925
DMSO	Sigma-Aldrich	Cat# D2650
Dextran from Leuconostoc spp.	Sigma-Aldrich	Cat# 31392-250G
Poly(vinyl alcohol)	Sigma-Aldrich	Cat# P1763

(Continued on next page)

**Continued**

REAGENT or RESOURCE	SOURCE	IDENTIFIER
Sodium chloride	Carl-Roth	Cat# P029.2
EDTA	Sigma-Aldrich	Cat# 03690
Fetal Bovine Serum (low endotoxin)	Sigma-Aldrich	Cat# F7524
Fetal Bovine Serum	Sigma-Aldrich	Cat# S0615
Ficoll-Paque	GE Healthcare	Cat# 17-1440-03
Biocoll®, Separation solution 1,077 g/mL isoton	Bio-sell	Cat# BS.L6115
G-CSF, Lenograstim	Italfarmaco spa	N/A
Human GM-CSF, premium grade	Miltenyi Biotec	Cat# 130-093-865
Human IL-4, premium grade	Miltenyi Biotec	Cat# 130-093-921
Human Serum, heat inactivated	Sigma-Aldrich	Cat# H4522
Human Serum AB pool, heat inactivated	University Department Essen/Transfusion medicine	N/A
LPS-EB Ultrapure	InvivoGen	Cat# tlrl-3pelps
R848 (Resiquimod)	InvivoGen	Cat# tlrl-r848
Recombinant human IL-2	PREPOTHEC	Cat# 200-02
Sodium chloride solution, 5 M	Sigma-Aldrich	Cat# S5150-1L
PMA	Sigma-Aldrich	Cat# P8139
Propidium Iodide	Sigma-Aldrich	Cat# P4864
Sytox-AAdvanced Dead Cell Stain	Invitrogen	Cat# S10349
RPMI 1640, 1X	Corning	Cat# 15-040-CV
Vybrant DyeCycle Violet	ThermoFisher scientific	Cat# V35003
eBioscience™ Fixable Viability Dye eFluor® 660	ThermoFisher scientific	Cat# 65-0864-14
L-Glutamine 100X	Biowest	Cat# X0550-100
Penicillin-Streptomycin solution 100X	Biowest	Cat# L0022-100
2-Mercaptoethanol	Sigma-Aldrich	M3148-25mL

**Critical commercial assay**

Anti-FITC MicroBeads	Miltenyi Biotec	Cat# 130-048-701
CD14 MicroBeads, human	Miltenyi Biotec	Cat# 130-050-201
NK cell isolation kit, human	Miltenyi Biotec	Cat# 130-092-657
Pan T cell isolation kit, human	Miltenyi Biotec	Cat# 130-096-535
BD Rhapsody Cartridge Kit	Becton Dickinson	Cat# 633733
BD Rhapsody cDNA Kit	Becton Dickinson	Cat# 633773
BD Rhapsody WTA Amplification Kit	Becton Dickinson	Cat# 633801
High Sensitivity D5000 ScreenTape	Agilent	Cat# 5067-5592
Human Single-Cell Multiplexing Kit	Becton Dickinson	Cat# 633781
NextSeq 500/550 High Output Kit v2.5 (150 Cycles)	Illumina	Cat# 20024907
NextSeq 500/550 High Output v2 kit (75 cycles)	Illumina	Cat# 20024906
Quant-iT™ RiboGreen® RNA Assay Kit	Thermo Fisher	Cat# R11490
Qubit dsDNA HS Assay Kit	Thermo Fisher	Cat# Q32854
RNase-free DNase set	QIAGEN	Cat# 79254
RNeasy Mini Kit	QIAGEN	Cat# 74104

**Deposited Data**

Bulk RNA-seq data of mLDG from SLE patients	Mistry et al. <sup>9</sup>	GEO: GSE13936
Bulk RNA-seq data of neutrophils activated with R848	Tamassia et al. <sup>70</sup>	GEO: GSE119394
Bulk RNA-seq data	This study	GEO: GSE250002 subseries GSE191254
scRNA-seq data	This study	GEO: GSE250002 subseries GSE250001
scRNA-seq data of TANs and NANs	Salcher et al. <sup>29</sup>	CZ CELLxGENE Discover: <a href="https://cellxgene.cziscience.com/collections/edb893ee-4066-4128-9aec-5eb2b03f8287">https://cellxgene.cziscience.com/collections/edb893ee-4066-4128-9aec-5eb2b03f8287</a>

(Continued on next page)

**Continued**

REAGENT or RESOURCE	SOURCE	IDENTIFIER
Bulk RNA-seq and scRNA-seq data of neutrophil precursors from BM of HD	Calzetti et al. <sup>32</sup>	GEO: GSE164687
Metadata of scRNA-seq data of TANs	Zilionis et al. <sup>30</sup>	GEO: GSE12746
<b>Oligonucleotides</b>		
ISPCR	Picelli et al. <sup>71</sup> ThermoFisher	N/A
Oligo-dT	Picelli et al. <sup>71</sup> ThermoFisher	N/A
Template-switching oligo (TSO)	Picelli et al. <sup>71</sup> Exiqon	N/A
Primers for mRNA expression, see <a href="#">STAR Methods</a>	This study	N/A
<b>Software and algorithms</b>		
Bcl2fastq2 version 2.20	Illumina	<a href="https://emea.support.illumina.com/downloads/bcl2fastq-conversion-software-v2-20.html">https://emea.support.illumina.com/downloads/bcl2fastq-conversion-software-v2-20.html</a>
Trim Galore! version 0.5.0		<a href="https://www.bioinformatics.babraham.ac.uk/projects/trim_galore/">https://www.bioinformatics.babraham.ac.uk/projects/trim_galore/</a>
HISAT2 version 2.1.0	Kim et al. <sup>72</sup>	<a href="http://daehwankimlab.github.io/hisat2/">http://daehwankimlab.github.io/hisat2/</a>
HTSeq-count version 0.11.0	Anders et al. <sup>73</sup>	<a href="http://www-huber.embl.de/HTSeq">http://www-huber.embl.de/HTSeq</a>
DESeq2 version 1.22.2	Love et al. <sup>74</sup>	<a href="https://bioconductor.org/packages/release/bioc/html/DESeq2.html">https://bioconductor.org/packages/release/bioc/html/DESeq2.html</a>
RUVSeq version 1.16.1	Risso et al. <sup>75</sup>	<a href="https://bioconductor.org/packages/release/bioc/html/RUVSeq.html">https://bioconductor.org/packages/release/bioc/html/RUVSeq.html</a>
matrixStats version 0.58.0		<a href="https://cran.rstudio.com/web/packages/matrixStats">https://cran.rstudio.com/web/packages/matrixStats</a>
PCAtools version 2.2.0		<a href="https://www.bioconductor.org/packages/release/bioc/html/PCAtools.html">https://www.bioconductor.org/packages/release/bioc/html/PCAtools.html</a>
factoextra version 1.0.7		<a href="https://cran.r-project.org/web/packages/factoextra">https://cran.r-project.org/web/packages/factoextra</a>
GeneOverlap version 1.20.0		<a href="https://bioconductor.org/packages/release/bioc/html/GeneOverlap.html">https://bioconductor.org/packages/release/bioc/html/GeneOverlap.html</a>
PANTHER16.0	Mi et al. <sup>76</sup>	<a href="http://pantherdb.org/webservices/go">http://pantherdb.org/webservices/go</a>
REVIGO	Supek et al. <sup>77</sup>	<a href="http://revigo.irb.hr/">http://revigo.irb.hr/</a>
R Studio and R environment	The R project for Statistical Computing	<a href="https://rstudio.com/">https://rstudio.com/</a> and <a href="https://cran.r-project.org/">https://cran.r-project.org/</a>
DoRothEA version 1.8.0	Garcia-Alonso et al. <sup>21</sup>	<a href="https://bioconductor.org/packages/release/data/experiment/html/dorothea.html">https://bioconductor.org/packages/release/data/experiment/html/dorothea.html</a>
SevenBridges	Seven Bridges Genomics Inc.	<a href="https://www.sevenbridges.com">https://www.sevenbridges.com</a>
QIAGEN IPA	Krämer et al. <sup>78</sup>	<a href="https://digitalinsights.qiagen.com/IPA">https://digitalinsights.qiagen.com/IPA</a>
Seurat version 4.1.1	Hao et al. <sup>79</sup>	<a href="https://satijalab.org/seurat/">https://satijalab.org/seurat/</a>
harmony version 0.1.0	Korsunsky et al. <sup>80</sup>	<a href="https://portals.broadinstitute.org/harmony/">https://portals.broadinstitute.org/harmony/</a>
UCell version 2.4.0	Andreatta et al. <sup>81</sup>	<a href="https://bioconductor.org/packages/release/bioc/html/UCell.html">https://bioconductor.org/packages/release/bioc/html/UCell.html</a>
sva version 3.48.0	Leek et al. <sup>82</sup>	<a href="https://www.bioconductor.org/packages/release/bioc/html/sva.html">https://www.bioconductor.org/packages/release/bioc/html/sva.html</a>
GraphPad Prism version 9	GraphPad Software, Inc	<a href="http://www.graphpad.com/scientific-software/prism/">http://www.graphpad.com/scientific-software/prism/</a>
FlowJo™ version 10.8.1	Becton, Dickinson, and Company; 2021	<a href="https://www.flowjo.com/solutions/flowjo">https://www.flowjo.com/solutions/flowjo</a>
CorelDraw Graphics Suite 2020	COREL™	<a href="https://www.coreldraw.com">https://www.coreldraw.com</a>
Inkscape version 1.2	Inkscape Project. (2020)	<a href="https://inkscape.org/">https://inkscape.org/</a>

## RESOURCE AVAILABILITY

### Lead contact

Further information and requests for resources and reagents should be directed to and will be fulfilled by the lead contact, Patrizia Scapini ([patrizia.scapini@univr.it](mailto:patrizia.scapini@univr.it)).

### Materials availability

This study did not generate new unique reagents.

### Data and code availability

- (1) Bulk RNA-seq and scRNA-seq data generated in this study have been deposited at Gene Expression Omnibus database (<https://www.ncbi.nlm.nih.gov/geo/>) and are publicly available as of the date of publication. Accession numbers are listed in the [key resources table](#).
- (2) This paper does not report original code.
- (3) Any additional information required to reanalyze the data reported in this paper is available from the [lead contact](#) upon request.

## EXPERIMENTAL MODEL AND STUDY PARTICIPANT DETAILS

### Study participants

**Lab 1 (University of Verona, Verona, Italy).** Peripheral blood was collected from: i) GDs, peripheral blood stem cell donors receiving 8–10  $\mu\text{g/kg/day}$  rh G-CSF (Lenograstim, Italfarmaco, Italy) for 5 days ( $n = 27$ ; [Table S1](#)), selected according to the “Italian bone marrow donor registry” criteria, and based on their HLA-compatibility with related or unrelated recipients; ii) NSCLC patients ( $n = 29$ ; [Table S1](#)); iii) breast cancer patients ( $n = 8$ ; [Table S2](#)); iv) DLBCL patients ( $n = 4$ ; [Table S2](#)); v) gender and age-matched HDs ( $n = 28$ ; [Table S1](#)), offering their blood to the Blood Bank Unit of the Verona “Azienda Ospedaliera Universitaria Integrata (AOUI)”. For selected experiments, BM aspirates were also obtained from healthy donors (HDs,  $n = 10$ ; [Table S1](#)) according to the IBMDR criteria.

**Lab 2 (University of Duisburg-Essen, Essen, Germany).** Peripheral blood was collected from patients with primary HNC ( $n = 65$ ; [Table S1](#)), RCC ( $n = 11$ ; [Table S2](#)), TCC ( $n = 13$ ; [Table S2](#)) and from gender and age-matched HDs ( $n = 13$ ; [Table S1](#)).

Criteria for patients’ selection were: 18 years or older patients; no systemic glucocorticoids and/or immunosuppressive treatment; no active infective and/or autoimmune diseases; no ongoing radio- or chemo- or immunotherapy. See [Tables S1](#) and [S2](#) for detailed characteristics of cancer patients. In selected experiments, NSCLC patients receiving immune checkpoint inhibitors (ICIs; such as pembrolizumab, nivolumab, durvalumab or atezolizumab) were enrolled before initiating ICI treatment (t0) and during clinical check-up (post - therapy). Similarly, HNC patients were enrolled before starting different types of therapies, including surgery, radiochemotherapy, surgery *plus* radiotherapy or surgery *plus* radiochemotherapy (t0), and during clinical check-up (post - therapies).

The study has been conducted according to the Declaration of Helsinki principles and cleared by the Ethic Committee of the Azienda Ospedaliera Universitaria Integrata di Verona (Italy) (CMRI/55742) and the Ethics committee of the Medical Faculty of the University of Duisburg-Essen. All patients signed informed consent forms.

### Cell lines and primary cells

K562 cells were cultured in RPMI-1640 medium supplemented with 10% FBS (SigmaAldrich), 1% ultraglutamine and 1% penicillin/streptomycin (Biowest). Cells were seeded at 0.1 million/mL density and passaged or harvested at around 0.75 million/mL density (75% confluence).

Primary cells utilized in this study (LDNs/PMN-MDSCs and NDNs, T cells, monocytes and NK cells) were isolated from blood samples from study participants, collected in EDTA - or sodium citrate - treated tubes by venipuncture and processed within 1 h. In selected experiments LDNs/PMN-MDSCs and NDNs were collected also from fresh BM aspirate samples - 1.5/2 mL - collected under aseptic conditions in a heparinized sterile syringe. Mononuclear cells and granulocytes were separated by density gradient centrifugation of blood onto either Ficoll-Paque (GE Healthcare; University of Verona) or Biocoll (Merk Millipore; University of Duisburg-Essen).<sup>12,14</sup> LDNs/PMN-MDSCs were isolated from the mononuclear cell fraction, while NDNs were isolated from the granulocyte fraction, by either cell sorting by flow cytometry or magnetic bead selection.<sup>12,14</sup> More details on the isolation procedures of LDNs/PMN-MDSCs and NDNs are reported in the METHOD DETAIL section.

CD2<sup>+</sup>CD3<sup>+</sup>CD5<sup>+</sup>CD7<sup>+</sup> T cells, CD14<sup>+</sup> monocytes and NK cells were isolated by Pan T cell Isolation kit II, CD14<sup>+</sup> Microbeads Kits, and NK cell isolation kit II (all from Miltenyi Biotec), respectively, from the mononuclear cell fractions of randomly selected HDs. Purity of cell preparation were higher than 95%. CD14<sup>+</sup> monocytes and NK cells were immediately used for proliferation or cytotoxicity assay, T cells were stored in liquid nitrogen until use.

## METHOD DETAILS

### Cell isolation and culture

For cell sorting by flow cytometry, mononuclear cells or granulocytes were incubated with neutrophil specific antibodies as described in the flow cytometry section, and sorted using either a FACS Aria II flow cytometer (Becton Dickinson; University of Verona) or a BD FACS Aria III Cell Sorter (BD Bioscience, IMCES, University of Duisburg-Essen).<sup>12,14</sup> Isolation of total CD66b<sup>+</sup> neutrophils by magnetic bead selection was performed by incubating mononuclear cells or granulocytes with fluorescence-conjugated anti-CD66b mAbs, followed by incubation with specific anti-fluorochrome microbeads (Milteny Biotec).<sup>12</sup>

In selected experiments, mNDNs from HDs were isolated by utilizing the EasySep neutrophil enrichment kit (StemCell Technologies).<sup>70</sup> Purified mNDNs from HDs were suspended at  $5 \times 10^6$ /mL in RPMI 1640 medium supplemented with 10% low endotoxin FBS (<0.5 EU/mL; from Sigma-Aldrich), 1% ultraglutamine and 1% penicillin/streptomycin (Biowest) and treated or not with: 1,000 U/mL G-CSF (Myelostim, Italfarmaco Spa) for 20 h, 20 ng/mL GM-CSF (MiltenyBiotec) for 20 h, 1  $\mu$ g/mL LPS (ultrapure, Escherichia coli 0111:B4 strain, InvivoGen) for 4 h or with 5  $\mu$ M R848 (InvivoGen) for 6 or 20h, then seeded in 24-well tissue culture plates (Greiner Bio-One, Kremsm ster, Austria) and cultured at 37°C, 5% CO<sub>2</sub> atmosphere. After the desired incubation period, cells were collected and spun for 5 min at 300 x g and the cell pellets were extracted for total RNA using the RNeasy mini kit followed by DNase I treatment, according to the manufacturer's protocol (Qiagen) and processed for RNA sequencing or RT-qPCR.<sup>70</sup>

### Flow cytometry experiments

For flow cytometry experiments, typically  $2 \times 10^5$  cells were resuspended in 20  $\mu$ L of PBS (Corning) containing 2% FBS (Sigma-Aldrich) and 2 mM EDTA (Sigma-Aldrich) (from now on termed "staining buffer"), and subsequently incubated for 30 min at 4°C with 5% human serum (Sigma-Aldrich). Cells were then stained for 30 min at 4°C using the fluorochrome-conjugated monoclonal/polyclonal antibodies (mAbs/pAbs) listed in the [key resources table](#). For immunophenotypic characterization, data from 150,000 events were acquired by an eight-color three-laser MACSQuant 10 Analyzer or fourteen-color three-laser-MACSQuant 16 Analyzer (Milteny Biotec) in Verona, or by an eight-color three laser FACSCanto II and FACSDiva 9.0 software (BD Biosciences, Heidelberg, Germany) in Essen, while data analysis was performed using FlowJo software v10.7.1 (BD Bioscience). Phenotypic analysis was performed on live cells identified as Vybrant-negative (Vybrant DyeCycle Violet; ThermoFisher scientific), propidium iodide-negative (Merck Life Science), Sytox-AAAdvanced Dead Cell Stain Kit-negative (Invitrogen), or Fixable Viability Dye eFluor 450/eFluor660-negative (ThermoFisher scientific) cells. The delta median fluorescence intensity ( $\Delta$  MFI) relative to each marker was obtained by subtracting either the MFI of the correspondent isotype control or the cell autofluorescence (revealed as Fluorescence Minus One, FMO, control) from the MFI of the specific antibody.

### T cell proliferation assay

CD14<sup>+</sup> monocytes were differentiated into mature DCs (mDCs) *in vitro* with 50 ng/mL GM-CSF, 10 ng/mL IL-4 (Milteny Biotec) and 1  $\mu$ g/mL LPS,<sup>83</sup> and stored in liquid nitrogen until use. T cell proliferation assay was performed in 96-well plates pre-coated with 1  $\mu$ g/mL anti-CD3 mAbs [(UCHT1, R&D Systems) for 1 h at 37°C. T cells and autologous mDCs were thawed and rested at 37°C, 5% CO<sub>2</sub> overnight.  $4 \times 10^4$  T cells/well,  $1 \times 10^3$  mDCs/well and 2  $\mu$ g/mL anti-CD28 mAbs (CD28.2, Biolegend) were added to the plates and co-cultured with or without  $2 \times 10^5$  sorted CD66b<sup>+</sup>CD10<sup>+</sup>CD11b<sup>high</sup>CD16<sup>high</sup> mNDNs/mLNDNs from GDs or mNDNs from HDs.<sup>12</sup> Following a 96 h-incubation period the T cell proliferation was determined by BrDU incorporation by ELISA (Cell proliferation ELISA, Roche) or by the carboxyfluorescein diacetate succinimidyl ester (CFSE) dilution assays (CellTrace CFSE Cell Proliferation Kit, Life Technologies).<sup>12</sup> The purity of all sorted cells was always greater than 98%, as determined by flow cytometry.

### Cell cytotoxicity assay

K562 tumor cells ( $5 \times 10^3$ /well), previously labeled with 5-chloromethylfluoresceine diacetate (CellTraker Green CMFDA, Invitrogen), were suspended in 200  $\mu$ L of RPMI-1640 supplemented with 10% FBS, 1% ultraglutamine and 1% penicillin/streptomycin (Biowest) and cultured in 96-well plates. To test the capacity of neutrophils to inhibit NK cell cytotoxicity, freshly isolated NK cells (NK cell isolation kit II, Milteny Biotec; purity >95%) stimulated with 100 U/mL IL-2 (Proleukin)<sup>16</sup> were co-cultured with CMFDA-labeled K562 cells (at a 4 to 1 effector cell/target cell ratio) in the presence or the absence of sorted CD66b<sup>+</sup>CD10<sup>+</sup>CD11b<sup>high</sup>CD16<sup>high</sup> mNDNs/mLNDNs from GDs or mNDNs from HDs (1–10 NK cell/neutrophil ratio). After an overnight incubation, dead/live cell dyes were analyzed by propidium iodide (Merck Life Science) and Vybrant DyeCycle Violet (ThermoFisher scientific), respectively, to identify the percentage of tumor cell lysis by flow cytometry. Anti-human CD56 and anti-human CD66b monoclonal antibodies ([key resources table](#)) were added to distinguish NK cells and neutrophils, respectively, from CMFDA-labeled K562 cells.

To test neutrophil-mediated cytotoxicity, sorted CD66b<sup>+</sup>CD10<sup>+</sup>CD11b<sup>high</sup>CD16<sup>high</sup> mNDNs/mLNDNs from GDs or mNDNs from HDs were co-cultured for 24 h with CMFDA-labeled K562 cells (at a 40 to 1 effector cell/target cell ratio) in the presence or the absence of 2.5 ng/mL phorbol 12-myristate 13-acetate (PMA, Sigma-Aldrich) or (as control vehicle) 0.004% DMSO. The percentage of tumor cell lysis by flow cytometry was calculated as described above.



### RT-qPCR

Purified RNA was reverse-transcribed into cDNA using PrimeScript RT Reagent kit (Takara, Japan), while qPCR was carried out using TB green premix Ex Taq (Takara, Japan).<sup>70</sup> Sequences of gene-specific primer pairs (Life Technologies) are the following: *PPIB* forward 5'-GGTGATCTTTGGTCTCTTCGG-3' and reverse 5'-TAGATGCTCTTCTCCTGTG-3'; *OLR1* forward 5'-CATGCAATTATCC CAGGTGTC-3' and reverse 5'-GGATTCTCATTACAGCTTCCGA-3'; *CD52* forward 5'-TGGTACAGATACAACTGGACTC-3' and reverse 5'-AAGCAGAAGAGGTGGATTATGG-3'; *CD84* forward 5'-TAACACCAGGAGACTCAGAAAC-3' and reverse 5'-CCAAGCC GACGATAGATTTC-3'; *PTGER2* forward 5'-AGACGGACCACCTATTCTC-3' and reverse 5'-AACGCATTAGTCTCAGAACAGG-3'; *LAI1* forward 5'-TCACAATGAGCATGCACCTG-3' and reverse 5'-TCTCTGTCTTCTCAGGAAGTC-3'. Data were calculated by Q-Gen software (<https://www.gene-quantification.de/download.html>) and expressed as mean normalized expression (MNE) units after *PPIB* normalization.

### RNA sequencing (RNA-seq)

**Lab 1 (University of Verona, Verona, Italy).** Cellular samples purified for RNA-seq experiments were: i) circulating CD66b<sup>+</sup>CD10<sup>+</sup>CD11b<sup>high</sup>CD16<sup>high</sup> mLDNs (n = 8) and mNDNs (n = 11) from GDs and control mNDNs (n = 10) from HDs; ii) CD66b<sup>+</sup>CD10<sup>+</sup>CD11b<sup>+</sup>CD16<sup>+</sup> BCs, CD66b<sup>+</sup>CD10<sup>+</sup>CD11b<sup>+</sup>CD16<sup>dim</sup> MMs, CD66b<sup>+</sup>CD10<sup>+</sup>CD11b<sup>dim</sup>CD16<sup>+</sup> MYs and CD66b<sup>+</sup>CD10<sup>+</sup>CD11b<sup>+</sup>CD16<sup>+</sup> PMs from either the peripheral blood of GDs (n = 4) or the BM of HDs (n = 3), all of them isolated by flow cytometry sorting (Figures S2A and S2D); iii) CD66b<sup>+</sup>CD10<sup>+</sup>CD11b<sup>high</sup>CD16<sup>high</sup> mPMN-MDSCs (n = 3) and autologous mNDNs (n = 3) from NSCLC patients, as well as control mNDNs from HDs (n = 3), were isolated from the peripheral blood by cell sorting via CD66b<sup>+</sup> beads<sup>12</sup> (Figure S2C) due to the small amount of blood available (<3 mL).

**Lab 2 (University of Duisburg-Essen, Essen, Germany).** Cellular samples purified for RNA-seq experiments were CD66b<sup>+</sup>CD10<sup>+</sup>CD11b<sup>high</sup>CD16<sup>high</sup> mNDNs (n = 5) and mPMN-MDSCs (n = 5) from HNC patients, as well as control mNDNs from HDs (n = 4), all of them isolated from the peripheral blood by flow cytometry sorting<sup>14</sup> (Figure S2B).

In selected experiments, RNA-seq experiments were also performed with: i) mNDNs from HDs stimulated or not with G-CSF, GM-CSF, R848 or LPS *in vitro* as described above (prepared in Lab 1); ii) CD16<sup>high</sup>CD62L<sup>high</sup> (n = 3) and CD16<sup>high</sup>CD62L<sup>low</sup> (n = 3) neutrophils purified from healthy donors receiving 2 ng/kg LPS for 3 h in collaboration with Prof. Leo Koenderman's lab (University Medical Center Utrecht, Utrecht, The Netherlands).<sup>28</sup>

Notably, the purity of all sorted mature and immature neutrophil populations ranged from 91 to 99.9%, as determined by flow cytometry. The RNA-seq libraries of all the cellular samples were prepared using the Smart-seq2 protocol<sup>70,71</sup> except for the RNA-seq libraries of mNDNs from HDs stimulated with LPS *in vitro* that were prepared using the Illumina TruSeq RNA SamplePrep Kit (Illumina, San Diego, CA, USA).

### RNA-seq library preparation

Total RNA was extracted after cell lysis by the RNeasy Mini Kit (QIAGEN, Venlo, Limburg, Netherlands). An on-column DNase digestion with the RNase-free DNase set (QIAGEN) was performed during total RNA isolation, to completely remove any possible contaminating DNA. RNA-seq libraries of cellular samples from (i) the peripheral blood of GD donors, HNC, NSCLC patients, LPS-treated donors and related HDs, (ii) BM aspirates of HDs<sup>32</sup> and (iii) mNDNs from HDs, incubated *in vitro* with or without G-CSF, GM-CSF or R848,<sup>70</sup> were prepared using the Smart-seq2 protocol.<sup>70,71</sup> For preparation of RNA-seq libraries, 2 ng of total RNA were copied into first strand cDNA by reverse transcription and template-switching oligo (dT) primers and an LNA-containing template-switching oligo (TSO). The resulting cDNA was pre-amplified, purified, and tagged with Tn5 transposase (kindly gifted by Dr. Sebastiano Pasqualato, European Institute of Oncology, Milan, 20139, Italy). cDNA fragments generated after tagmentation were gap-repaired, enriched by PCR and purified to create the final cDNA library. Libraries were sequenced on the Illumina NextSeq 500. RNA-seq libraries of mNDNs from HDs stimulated with LPS *in vitro* were prepared using the Illumina TruSeq RNA SamplePrep Kit (Illumina, San Diego, CA, USA) and sequenced on the Illumina NextSeq 2000.

RNA-seq data of published studies were downloaded from the Gene Expression Omnibus (GEO) database. Specifically, we retrieved data related to: (i) mature low-density granulocytes (mLDGs) from SLE patients [GSE139360,<sup>9</sup>]; (ii) neutrophils activated *in vitro* with R848 [GSE119394,<sup>70</sup>]; and (iii) neutrophil precursors from BM aspirates of HDs [GSE164687,<sup>32</sup>].

### RNA-seq computational analysis

Computational analysis of transcriptomic datasets generated has been performed by the following bioinformatic pipeline. FASTQ files were generated from BCL data using bcl2fastq v2.20 software. After quality filtering, according to the Illumina pipeline, adapters and base quality trimming were performed using Trim Galore! v0.5.0 ([https://www.bioinformatics.babraham.ac.uk/projects/trim\\_galore/](https://www.bioinformatics.babraham.ac.uk/projects/trim_galore/)) with parameters -length 50, -three\_prime\_clip\_R1 3. Reads were aligned to the human genome GrCh38, previously downloaded from Ensemble release 94, using HISAT2 v2.1.0<sup>72</sup> for single-end reads or pair-end reads, as appropriate. Summed exon reads count per gene were estimated using HTSeq-count v0.11.0<sup>73</sup> with parameters -m intersection-nonempty, -t exon -i gene\_id, and normalized among various cellular samples by using DESeq2 v1.22.2,<sup>74</sup> but only protein coding genes were retained for downstream analysis. Prior to subsequent analysis, when necessary, batch effects were removed by using the RUVr function of RUVSeq v1.16.1<sup>75</sup> with residuals obtained according to type = deviance. Fragment per kilobase of transcript per million mapped reads (FPKM) and variance stabilized transformed data (vsd) were estimated by using the fpkm and vst functions of DESeq2,

respectively. Most variable genes were identified as genes having the higher variance of expression among all analyzed cellular samples, as calculated using the rowVars function of the matrixStats v0.58.0 package in R. Differentially expressed genes (DEGs) were identified by using the likelihood ratio test (LRT) or the Wald test, as appropriate, implemented in DESeq2, and using as selection parameter the Benjamini and Hochberg adjusted p value lower than 0.05. In selected analysis, gene expression is shown as  $\log_2$  (fold change) relative to gene expression in mNDNs from HDs, as obtained from DESeq2. Only protein coding genes significantly upregulated [Benjamini and Hochberg adjusted p value lower than 0.05 and  $\log_2$  (fold change) higher than 0] by G-CSF, GM-CSF, LPS or R848 stimulation, as compared to untreated cells, were used for subsequent analysis. The 500 most variable genes were used for hierarchical clustering and PCA. Hierarchical clustering was performed by using the Ward.D2 agglomerative algorithm on the Euclidean distance matrix, while PCA was performed using the PCAtools v2.2.0 package in R.

### K-means clustering and cluster overlap analysis

K-means clustering analysis was performed on the DEGs identified in mNDNs/mLNDNs from GDs versus group-related mNDNs from HDs, as well as on mPMN-MDSCs/mNDNs from NSCLC/HNC patients versus group-related mNDNs from HDs. FPKM expression values were Z score transformed and subjected to K-means clustering with optimal K determined according to the Shiloutte method implemented in the fviz\_nbclust function of the factoextra v1.0.7 package. Overlap between clusters of different experimental settings was obtained using the newGOM function of the GeneOverlap v1.20.0 package. Specifically, significance of the overlap was evaluated by a Fisher's exact test considering p value <0.05 as significant, while Jaccard Index was calculated to measure clusters similarity.

### Analysis of TF regulons and upstream regulators

To assess the existence of specific transcriptional regulatory networks associated with the defined mPMN-MDSC gene signature, we used DoRothEA,<sup>21</sup> a collection of resources of transcription factor (TF)'s targets (regulons), curated and collected from different type of evidence (Chip-Seq peaks, TF binding motifs, literature-curated resources) for both mice and humans, that can serve as gene sets for TF activity inference. Each TF is associated to a confidence level, ranging from A to E, based on the evidence supporting the interactions of the TF-target gene.

To estimate the TF regulon activity enrichment for the mPMN-MDSC gene signature, we used run\_viper function of DoRothEA v1.8 R package, a wrapper for VIPER function<sup>22</sup> which performs inference of protein activity using DoRothEA regulons.<sup>21</sup> Only more validated DoRothEA regulons, with confidence level A, B and C, were selected for the analysis.

The input gene list for run\_viper function was obtained calculating the average fold change of all the up-regulated genes belonging to the mPMN-MDSC gene signature and the down-regulated genes obtained from the previously described DEG analysis between the different mPMN-MDSC populations (mNDNs/mLNDNs from GDs; mPMN-MDSCs from NSCLC or HNC patients) and the relative controls (mNDNs from HDs; mNDNs from NSCLC or HNC patients). We then selected the top 25 positively enriched TF regulons and calculated their activity score across cellular samples and replicates starting from normalized counts using the run\_viper function with the scale method.<sup>21</sup>

To predict the upstream regulators, we used the commercial QIAGEN IPA (QIAGEN Inc., <https://digitalinsights.qiagen.com/IPA>)<sup>78</sup> software. Briefly, the average fold change of all the up-regulated genes belonging to the mPMN-MDSC gene signature was calculated and utilized for the following IPA analysis by setting the human species with relaxed filter.<sup>84</sup> We set the threshold at 0.05 to select the significant upstream regulators.

### Enrichment of the gene signature in bulk RNA-seq data

Gene signature specific for PMN-MDSCs<sup>15,19</sup> and mature low-density granulocytes (mLDGs) from SLE patients<sup>9</sup> were retrieved from published studies. Gene signature specific for CD16<sup>high</sup>CD62L<sup>low</sup> suppressive neutrophils purified from LPS-treated donors<sup>28</sup> were defined from differential gene expression analysis performed in this study and included only protein coding genes significantly more expressed [Benjamini and Hochberg adjusted p value lower than 0.05 and  $\log_2$  (fold change) higher than 0] in CD16<sup>high</sup>CD62L<sup>low</sup> suppressive neutrophils as compared to CD16<sup>high</sup>CD62L<sup>high</sup> non-suppressive neutrophils from LPS-treated donors. To test whether the mPMN-MDSC gene signatures were statistically enriched in PMN-MDSC, mLDG from SLE and CD62L<sup>low</sup> PMN gene signature the Fisher's exact test was used. P value lower than 0.05 was considered as significant.

### GO enrichment analysis

GO enrichment analysis was performed on the mPMN-MDSC gene signature for predicting biological process ontology domain (GO Ontology database <https://doi.org/10.5281/zenodo.4437524>, released 2021-01-01) by using PANTHER16.0.<sup>76,85</sup> Overrepresentation analysis was performed using the Fisher's exact test with FDR correction. Only GO terms with adjusted p values <0.05 were considered for subsequent analysis. Redundant GO terms were reduced by REVIGO<sup>77</sup> by using the SimRel semantic similarity measure and a cut-off of 0.5. GO terms having lower dispensability index and lower adjusted p values were plotted.

### Gene signature expression in neutrophil precursors

Neutrophil progenitors isolated from the peripheral blood of GDs and BM aspirates of HDs were compared in terms of mPMN-MDSC gene signature expression by applying a non-linear regression analysis. Briefly, for every leukocyte type the average FPKM value of

each signature gene was Z score transformed and used to build a second order polynomial model with least squares regression as fitting method. To test whether there was any evidence that GD and HD datasets differ from each other, curves were compared using the extra sum-of-squares F test. P value lower than 0.05 were considered statistically significant. For the analysis of the mPMN-MDSC gene signature expression in neutrophil progenitors, FPKM expression levels of genes composing the signature were Z score transformed and subjected to K-means clustering analysis with K = 25, as determined by the Gap statistic method implemented in the `fviz_nbclust` function of the `factoextra` package. Then, clusters with similar expression patterns across all the cellular samples were arranged into three main groups.

### Single-cell RNA-seq (scRNA-seq)

Total CD66b<sup>+</sup> neutrophils from the LDN and NDN fractions of peripheral blood from GDs and NSCLC patients, as well as from the NDN fraction of peripheral blood or the LDN fraction of BM from HDs as controls, were isolated by magnetic bead selection with fluorescence-conjugated anti-CD66b mAbs<sup>12</sup> and processed with BD Rhapsody Single-Cell Analysis System for scRNA-seq.<sup>32</sup>

### Seven Bridges processing for scRNA-seq data

After demultiplexing of bcl files by using Bcl2fastq2 v2.20 from Illumina and assessment of reads quality, paired-end scRNA-seq reads were filtered for valid cell barcodes using the barcode whitelist provided by BD. Then, sequenced reads were aligned to the hg38 human transcriptome and the expression of transcripts in each cell was quantified via the standard Rhapsody analysis pipeline (BD Biosciences) on Seven Bridges (<https://www.sevenbridges.com>), following manufacturer's recommendations.<sup>32</sup>

### Seurat workflow for scRNA-seq data analysis

The R package Seurat v4.1.1<sup>79</sup> was used for all downstream analysis. For each single dataset, cells were filtered<sup>32</sup> and contaminant non-neutrophil cells were removed, based on the expression of known marker genes. The different datasets were merged in two main groups: one composed by total CD66b<sup>+</sup> NDNs/LDNs from GDs (merged as a total of 23,453 cells; n = 6) and one composed by total CD66b<sup>+</sup> NDNs from HDs (6,070 cells; n = 7). To examine cell cycle variation was used the `CellCycleScoring` function which assigns a score to each cell based on its expression of G2/M and S phase markers. Normalization, detection of high variable genes and scaling were performed using the `SCTransform` function using as covariates the difference between the S and G2M cell cycle score and the percentage of mitochondrial UMIs. The PCA was performed on selected genes known to regulate neutrophil maturation.<sup>31</sup> To remove the batch effects across different donors we used the `RunHarmony` function of R package harmony v0.1.0<sup>80</sup> on the PCA data. The dimensional reduction was computed by summarizing the first 15 "harmony" components and visualized in a two-dimensional UMAP representation. The mature fraction of each dataset was assessed using a score computed by the `AddModuleScore` function setting as features DEGs highly expressed in the latest neutrophil maturation stage as described in the study by Grassi et al. [r2 cluster in Figure 1 of the study by Grassi et al. study<sup>31</sup> (see also Figures S3E and S3F)]. Cells with higher score (6,070 in mNDNs from HDs or 6,493 in mLDNs and 10,339 in mNDNs from GDs) were defined as mature neutrophils and merged in a dataset of mNDNs from HDs or mNDNs/mLDNs from GDs. The raw counts of the dataset were normalized as described above. The PCA was computed on 1,000 more variable genes. The batch correction and UMAP visualization were performed as before. The mPMN-MDSC gene signature and the short mPMN-MDSC gene signature scores were calculated using the `AddScoreModule` function or the `AddModuleScore_Ucell` function from UCell R package function, selecting for g1 only the top 150 DEGs, while including g2 and g3 entirely.

In selected experiments, total CD66b<sup>+</sup> NDNs/LDNs from GDs (as above), total CD66b<sup>+</sup> NDNs from HDs (as above), total CD66b<sup>+</sup> NDNs/PMN-MDSCs from NSCLC patients (8,494 cells; n = 3) and total CD66b<sup>+</sup> LDNs from HD BMs (5,781 cells, n = 2) were merged and normalized using the `Combat_Seq` function of the `sva` R package.<sup>82</sup> The dataset was then divided in two datasets: one containing total CD66b<sup>+</sup> NDNs/LDNs from GDs with control total CD66b<sup>+</sup> HD mature and immature neutrophils and one containing total CD66b<sup>+</sup> NDNs/PMN-MDSCs from NSCLC patients with control HD mature and immature neutrophils. The two datasets were clustered using the `FindCluster` function with resolution of 0.2 and the clusters were defined mature, or immature based on the presence or absence of mature neutrophils defined as above. The g1 gene signature score was calculated using the `AddModuleScore_Ucell` function from UCell R package.<sup>81</sup>

### Seurat workflow for published scRNA-seq datasets

Published TAN scRNA-seq datasets were retrieved from the large-scale NSCLC single cell atlas<sup>29</sup>: TAN and NAN datasets from the Salcher et al. study<sup>29</sup> were selected setting the following parameters: `dataset` = "UKIM-V" or "UKIM-V-2" and `ann_fine` = "Neutrophils"; TAN dataset from the Zilionis et al. study<sup>30</sup> were instead selected using the following settings: `dataset` = "Zilionis\_Klein\_2019" and `ann_fine` = "Neutrophils".<sup>29</sup> We integrated the datasets from the Salcher et al.<sup>29</sup> and the Zilionis et al.<sup>30</sup> studies using SCTransform integration workflow (<https://satijalab.org/seurat/v3.2/integration.html>), setting as reference dataset "UKIM-V-2". The PCA was performed using integrated assay. The dimensional reduction of the integrated dataset was computed by summarizing the first 20 principal components and visualized in a two-dimensional UMAP representation.

The cluster labels of the Zilionis et al.'s dataset<sup>30</sup> were retrieved from the metadata deposited in the NCBI GEO depository under the accession number GEO: GSE12746.

The UMAP region enriched in NANs or TANs was defined as "NAN-like cells" and "TAN-like cells", respectively. The mPMN-MDSC gene signature scores were computed as above.

NAN-like cells (n = 8842) and TAN-like cells (n = 7247) in the integrated dataset were defined using a score computed by the AddModuleScore function setting as features the DEGs belonging to the NAN or TAN signature defined in the study by Salcher et al.<sup>29</sup> (see also Figure 3B).

Published NCP scRNA-seq data were retrieved from the NCBI GEO repository (GEO: GSE164687). The NCP clusters c1, c2, c3, c4, defined in the study by Calzetti et al.,<sup>32</sup> were included in the analysis and we computed the score of the g1, g2 and g3 genes using the AddModuleScore function starting from DEGs in g1, g2 and g3 gene list, respectively.

## QUANTIFICATION AND STATISTICAL ANALYSIS

RNA-seq and scRNA-seq data statistical analysis were performed using R software v4.2 (The R project for Statistical Computing) as indicated.

For flow cytometry and RT-qPCR experiments, dataset distribution was evaluated using the Shapiro-Wilk normality test. According to normality test results, the comparison of variables was performed using the unpaired two-tailed Mann-Whitney test or the Wilcoxon matched-pairs signed rank test (for comparison between two groups) and either the Friedman or the Kruskal-Wallis test followed by pairwise either Dunn's or Wilcoxon's test (for comparison between three or more groups).

P-values lower than 0.05 were considered significant and asterisks indicate significant increases: \* = p value <0.05; \*\* = p value <0.01; \*\*\* = p value <0.001; \*\*\*\* = p value <0.0001. Graphs were elaborated using GraphPad Prism v9 software (GraphPad Software, Inc.).

**Supplemental information**

**Surface CD52, CD84, and PTGER2 mark  
mature PMN-MDSCs from cancer patients  
and G-CSF-treated donors**

**Francesca Pettinella, Barbara Mariotti, Chiara Lattanzi, Kirsten Bruderek, Marta Donini, Sara Costa, Olivia Marini, Giulia Iannoto, Sara Gasperini, Elena Caveggion, Monica Castellucci, Federica Calzetti, Francisco Bianchetto-Aguilera, Elisa Gardiman, Matteo Giani, Stefano Dusi, Maurizio Cantini, Aurora Vassanelli, Denise Pavone, Michele Milella, Sara Pilotto, Pamela Biondani, Benedikt Höing, Marie Carolin Schleupner, Timon Hussain, Boris Hadaschik, Cordelia Kaspar, Carlo Visco, Cristina Tecchio, Leo Koenderman, Flavia Bazzoni, Nicola Tamassia, Sven Brandau, Marco A. Cassatella, and Patrizia Scapini**



## SUPPLEMENTAL FIGURES AND TABLES

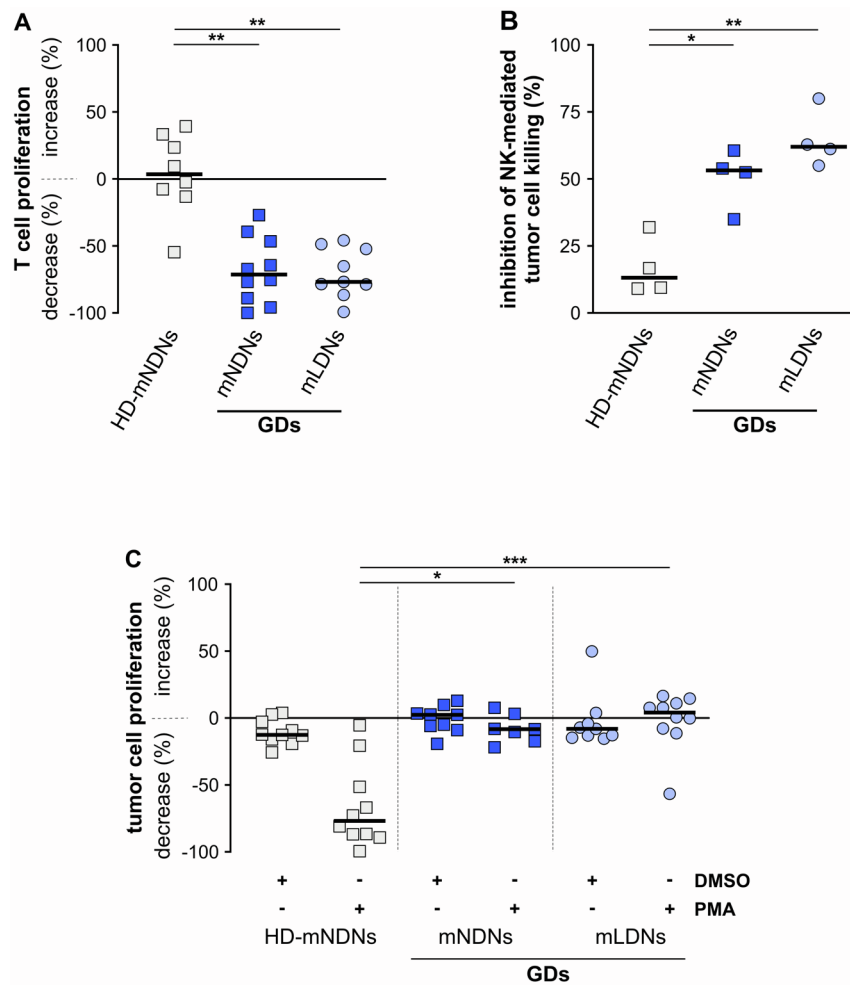


**Figure S1. mNDNs and mLDNs from GDs display functional PMN-MDSC activities at similar levels, related to STAR Methods.** (A and B) Effect on the proliferation of CD3/CD28-stimulated T cells (A,  $n = 8-10$ ), or on the killing of K562 tumor cells by NK cells (B,  $n = 4$ ), after their coculture with mNDNs/mLDNs from GDs or control mNDNs from HDs. (C) Effect on the proliferation of K562 tumor cells ( $n = 7-10$ ) induced by their coculture with mNDNs/mLDNs from GDs or control mNDNs from HDs incubated with 2.5 ng/mL PMA or (as control vehicle) 0.004% DMSO. Each symbol stands for a single HD or GD donor sample; \* $p < 0.05$ ; \*\* $p < 0.01$ ; \*\*\* $p < 0.001$ , by Kruskal-Wallis test followed by Dunn's multiple comparison test or Mann-Whitney test for all graphs. Median values from independent experiments are reported in the graphs.

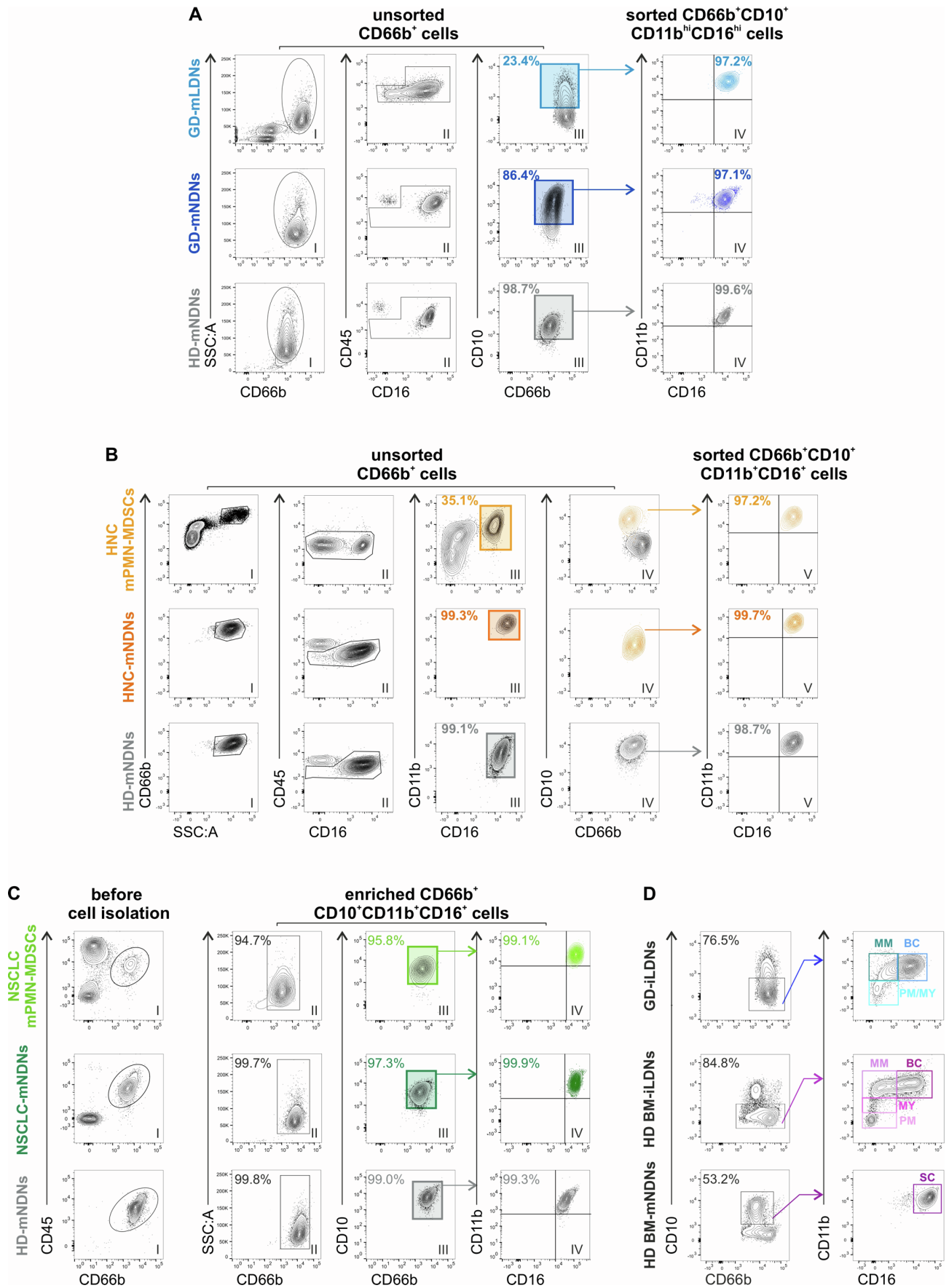


**Figure S2. Isolation of mature and/or immature LDNs and NDNs from GDs, cancer patients and HDs by flow cytometry sorting or magnetic bead selection, related to Figure 1, Figure 4 and STAR Methods. (A and B)** After gating on singlets, excluding debris and gating on  $CD45^+$  PI<sup>-</sup> cells (not shown): (A)  $CD66b^+CD10^+CD11b^{high}CD16^{high}$  mNDNs/mLNDNs from GDs and mNDNs from HDs were identified by: gating on total  $CD66b^+$  granulocytes (I), excluding

CD45<sup>high</sup>CD16<sup>-</sup> eosinophils (II) and finally gating on CD10<sup>+</sup> mNDNs/mLNDNs (III). All sorted cells displayed a CD66b<sup>+</sup>CD10<sup>+</sup>CD11b<sup>high</sup>CD16<sup>high</sup> phenotype (IV); **(B)** mPMN-MDSCs/mNDNs from HNC patients and mNDNs from HDs were identified by: gating on total SSC<sup>high</sup>CD66b<sup>high</sup> cells (I), excluding CD45<sup>high</sup>CD16<sup>-</sup> eosinophils (II) and gating on CD11b<sup>high</sup>CD16<sup>high</sup> mPMN-MDSCs/mNDNs (III). All sorted cells displayed a CD66b<sup>+</sup>CD10<sup>+</sup>CD11b<sup>high</sup>CD16<sup>high</sup> phenotype (IV). Panel (V) shows re-analysis of CD66b<sup>+</sup>CD16<sup>+/-</sup>CD11b<sup>+/-</sup> cells and expression of CD10<sup>+</sup>. **(C)** Representative flow cytometry plots displaying the purity of isolated mPMN-MDSCs/mNDNs from NSCLC patients and mNDNs from HDs, before (I) and after enrichment (II, III, IV) by magnetic bead selection. For these experiments, we selected NSCLC patients having a high frequency (> 96%) of CD66b<sup>+</sup>CD10<sup>+</sup>CD11b<sup>high</sup>CD16<sup>high</sup> mPMN-MDSCs within their total CD66b<sup>+</sup> PMN-MDSCs. **(D)** Representative flow cytometry plots displaying the gating strategies to identify and isolate CD66b<sup>+</sup>CD10<sup>-</sup>CD11b<sup>+</sup>CD16<sup>+</sup> band cells (BCs), CD66b<sup>+</sup>CD10<sup>-</sup>CD11b<sup>+</sup>CD16<sup>dim</sup> metamyelocytes (MMs), CD66b<sup>+</sup>CD10<sup>-</sup>CD11b<sup>dim</sup>CD16<sup>-</sup> myelocytes (MYs) and CD66b<sup>+</sup>CD10<sup>-</sup>CD11b<sup>-</sup>CD16<sup>-</sup> promyelocytes (PMs) from CD66b<sup>+</sup>CD10<sup>-</sup> iLDNs from either the peripheral blood of GDs (boxes in top right panel) or the BM of HDs (boxes in middle right panel). MYs and PMs from GDs were pooled by sorting total CD66b<sup>+</sup>CD10<sup>-</sup>CD11b<sup>dim/+</sup>CD16<sup>-</sup> cells to have sufficient cells for RNA-seq experiments. Gating strategy to identify and isolate CD66b<sup>+</sup>CD10<sup>+</sup> segmented cells (SCs) within NDNs from the HD BM is also reported (bottom panels).

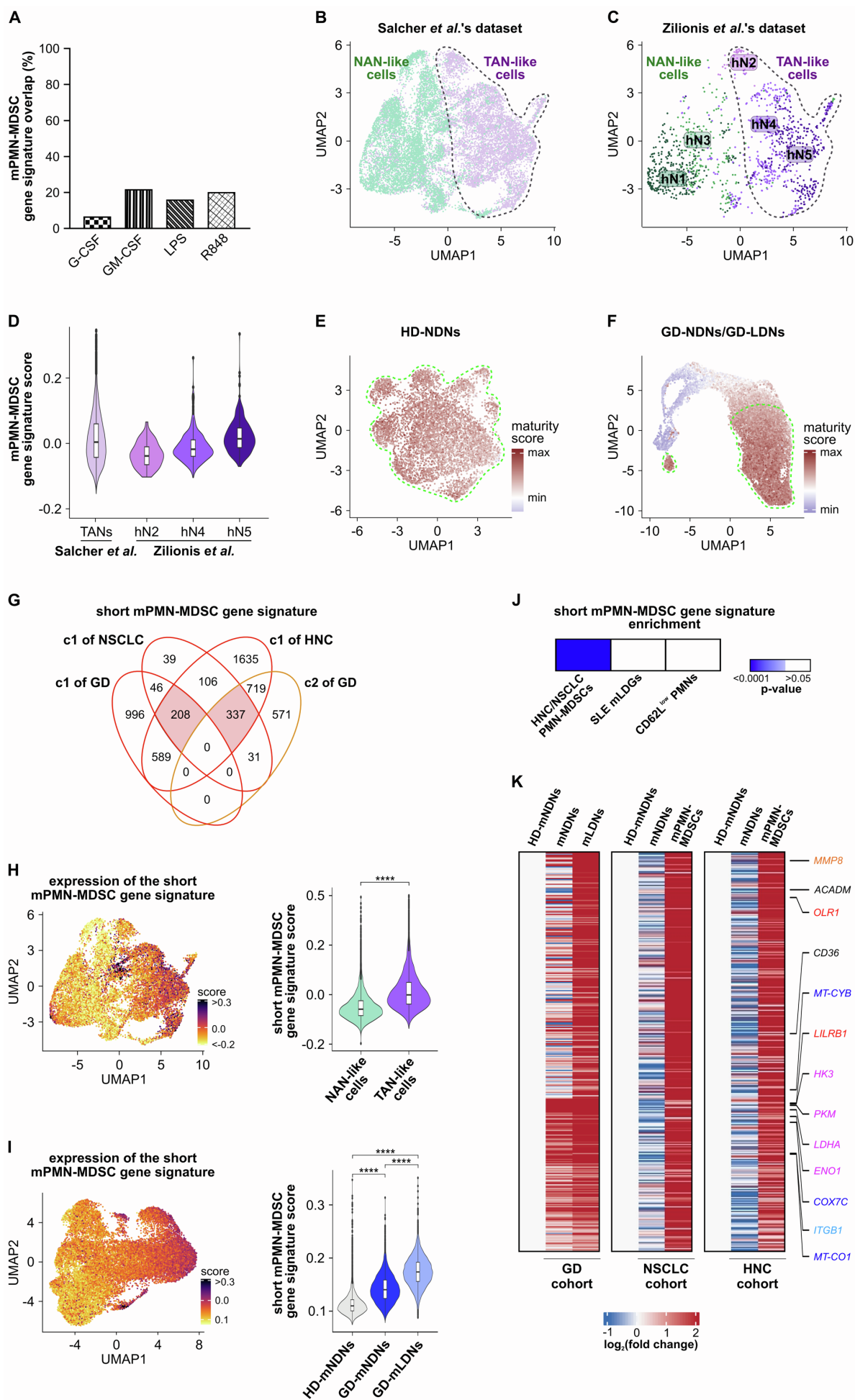


**Figure S3. Enrichment of the mPMN-MDSC gene signature in either mature neutrophil incubated *in vitro* with various agonists or in published TAN datasets. Identification and characterization of the short mPMN-MDSC signature, related to Figure 2 and 3.** (A) Percentages of the mPMN-MDSC gene signature accumulation in HD mNDNs incubated *in vitro* by 1000 U/mL G-CSF, 20 ng/mL GM-CSF, 1 µg/mL LPS or 5 µM R848. (B and C) UMAP plots of published NSCLC TAN and NAN datasets from the Salcher *et al.*'s study<sup>S1</sup> (B) or NSCLC TAN datasets from the Zilionis *et al.*'s study<sup>S2</sup> (C) showing the two main neutrophil populations defined in this study (as described in STAR Methods and in Figure 3B and 3C), namely NAN-like (green) and TAN-like (violet) cells. For the Zilionis *et al.*'s dataset,<sup>S2</sup> the TAN clusters defined in the original study (*h*N1-5) are reported. (D) Violin plots displaying the mPMN-MDSC gene signature scores across the TAN clusters identified in the Salcher *et al.*<sup>S1</sup> or the Zilionis *et al.*<sup>S2</sup>'s datasets. (E and F) Two-dimension UMAP representation of HD-NDNs (n = 7 donors; E) and merged NDNs/LDNs from GDs (n = 6 donors; F). For every cell, a maturity score was calculated evaluating the expression levels of a transcriptional module previously associated to neutrophils at their later stage of differentiation [i.e., cluster r2 of Figure 1 in<sup>S3</sup>]. The neutrophil populations with the highest maturity score are evidenced by the green boxes. (G) Venn diagram showing the number of genes shared between cluster 1 (c1) and c2 of the GD sample cohort, and c1 of both NSCLC and HNC sample cohorts. Intersections highlighted in dark pink were selected for the generation of the short mPMN-MDSC gene signature. (H and I) UMAP (H and I, left panels) and violin (H and I, right panels) plots of the score of short mPMN-MDSC gene signature calculated as normalized average expression of the genes composing the signature across NAN-like and TAN-like cells (H) or the HD/GD sample cohorts (I). \*\*\*\*p < 0.0001, by Kruskal-Wallis test followed by pairwise Wilcoxon test. (J) Enrichment of the short mPMN-MDSC gene signature in published gene signatures of PMN-MDSCs<sup>S4</sup> and mLDGs from SLE [SLE mLDGs<sup>S5</sup>] and suppressive CD16<sup>high</sup>CD62L<sup>low</sup> neutrophils (CD62L<sup>low</sup> PMNs) from LPS treated donors.<sup>S6</sup> Box colors correlate with the p-value for each comparison, calculated according to the Fisher's exact test. Data are shown as p-values according to the reported scale: white = non-significant enrichment (p > 0.05); shades of blue = significant enrichment (p < 0.05). (K) Heatmaps displaying the expression of the genes of the short mPMN-MDSC gene signature present in either mNDNs/mLDNs from GDs (left panel) or mPMN-MDSCs from NSCLC (middle panel) or HNC (right panel) patients. Data are represented as log<sub>2</sub> (fold change) relative to mNDNs from HDs. Selected genes are listed on the right of the heatmap. Font colors mean that those genes are included in the following biological process: black = metabolism; blue = ATP-metabolism; purple = glycolysis; orange = pro-angiogenic; light blue = epithelial to mesenchymal transition; red = PMN-MDSC-associated genes from literature.



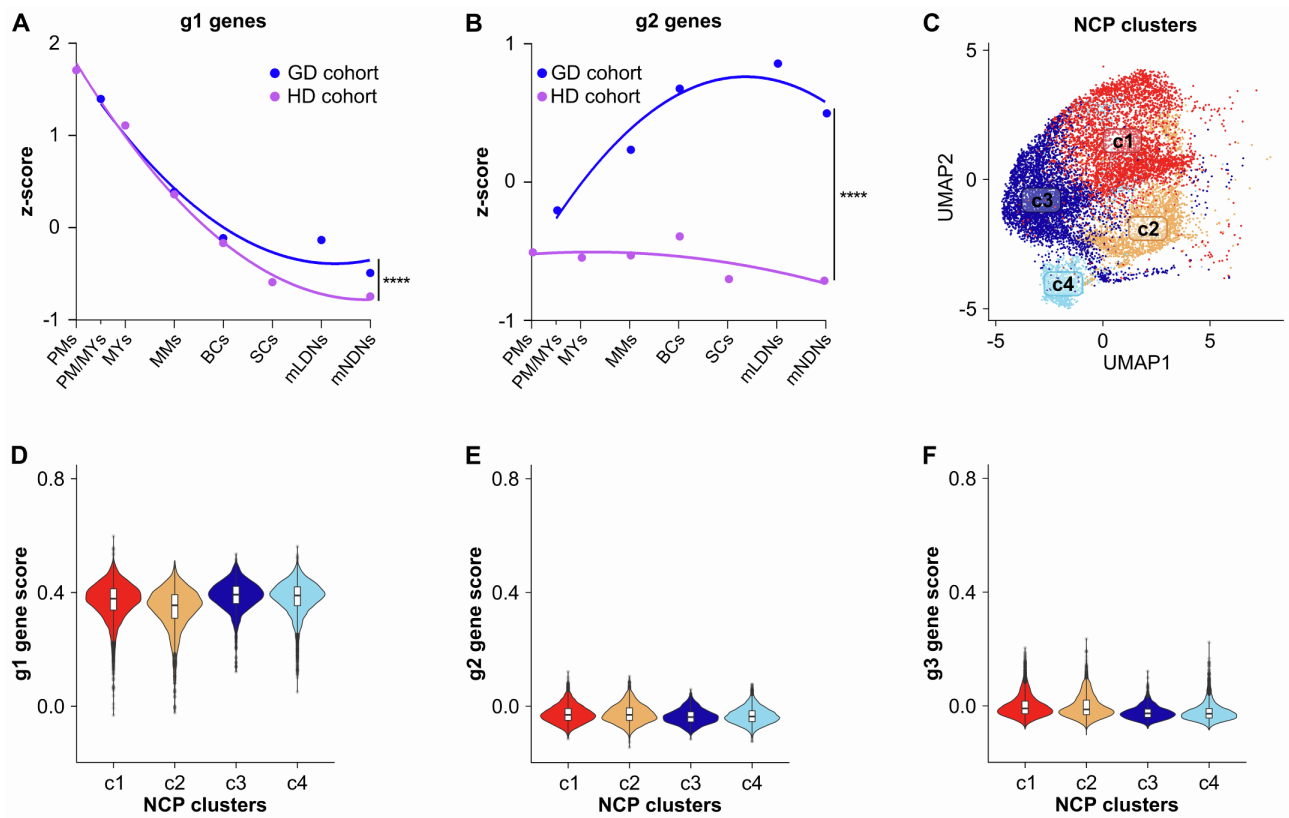


**Figure S4. Expression of g1, g2 and g3 genes of the mPMN-MDSC gene signature in either mature and immature neutrophils from GDs and HDs or in NCPs from HD BM, related to Figure 4.** (A and B) Average expressions of g1 (A) and g2 (B) genes in mature and immature neutrophils from GD and HD cohorts were fitted with a non-linear regression. Comparison of the GD versus HD regression curves was performed by the extra sum-of-squares F test. \*\*\*\* $p < 0.0001$ . (C–F) Two-dimension UMAP representation of NCP clusters from Calzetti *et al.* study<sup>S7</sup> (C). Violin plot displaying the g1 (D), g2 (E) and g3 (F) gene score across the NCP clusters.

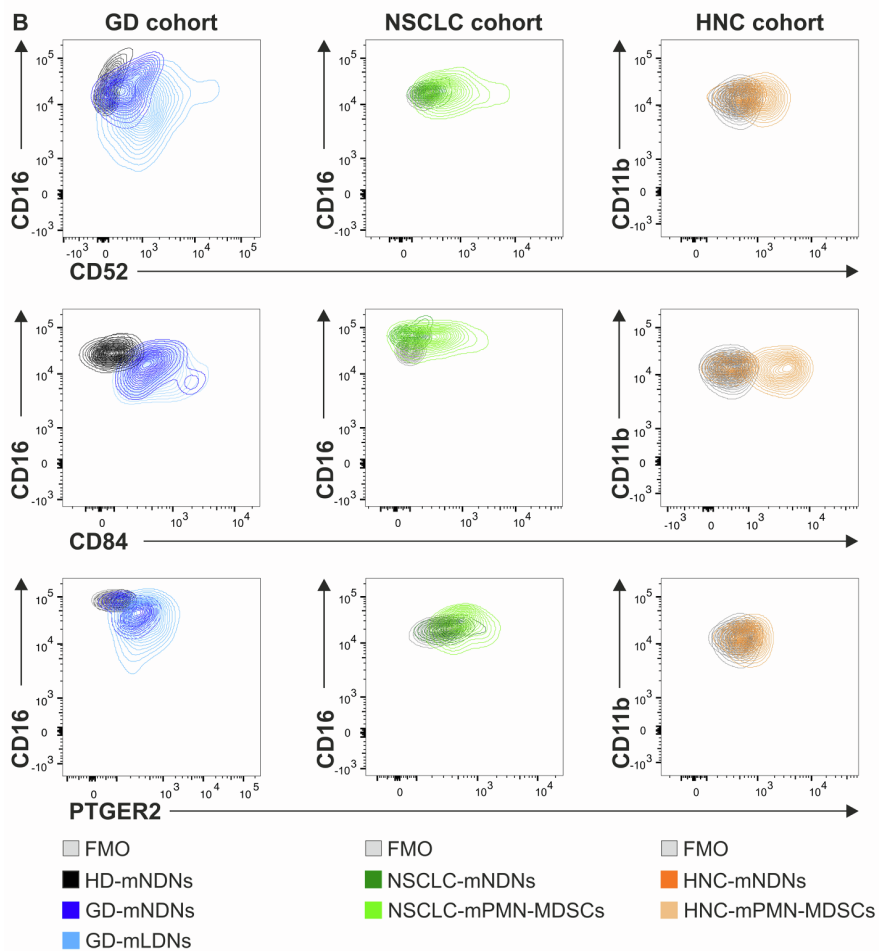
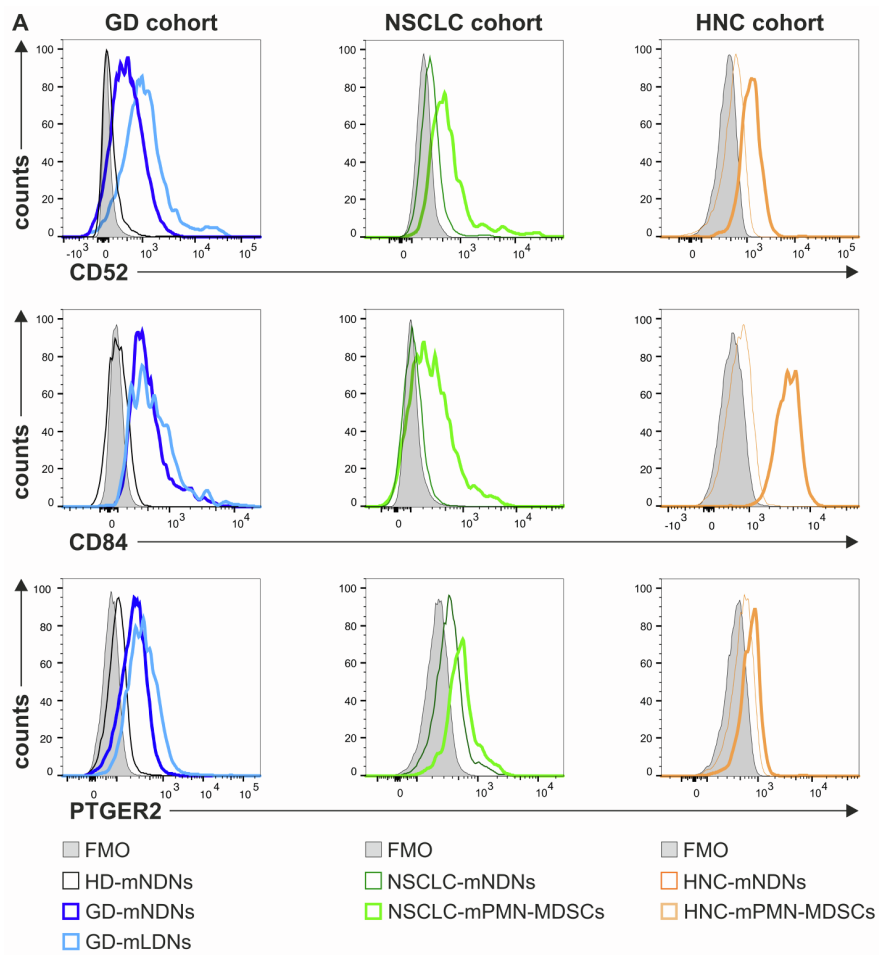


**Figure S5. CD52, CD84 and PTGER2 surface expression on mPMN-MDSCs from GDs and NSCLC/HNC patients, related to Figure 6.** Representative histogram (**A**) or contour plot (**B**) overlays showing the expression of surface CD52 (top panel rows), CD84 (middle panel rows) and PTGER2 (bottom panel rows) on: mNDNs/mLNDNs from GDs and control mNDNs from HDs (left panels); mPMN-MDSCs and autologous mNDNs from cohorts of patients with NSCLC (middle panels) or HNC (right panels). Grey histograms and contour plots correspond to fluorescence negative control. One representative experiment for each GD or cancer patient cohort is shown.

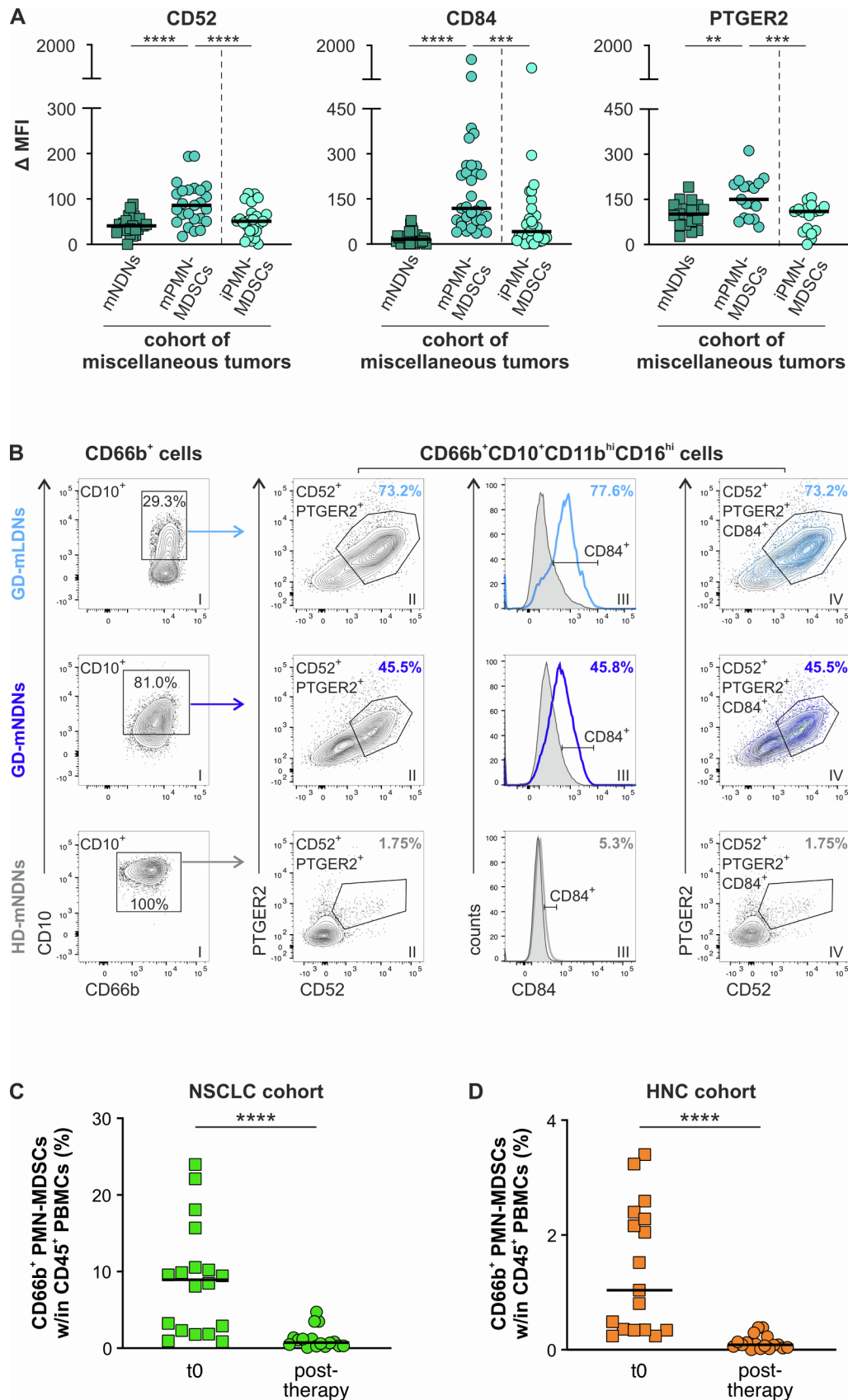


**Figure S6.** CD52, CD84 and PTGER2 surface expression on mPMN-MDSCs/iPMN-MDSCs from patients with miscellaneous tumors and CD52, CD84 and PTGER2 co-expression on mLDNs/mNDNs from GDs, related to **Figure 6**. (A) Surface CD52 (left panel), CD84 (middle panel) or PTGER2 (right panel) expression levels were evaluated by flow cytometry on mPMN-MDSCs/iPMN-MDSCs and autologous mNDNs from cohorts of patients with miscellaneous tumors (RCC, n = 3–11; breast cancer, n = 8–10; DLBCL, n = 4, TCC n = 3–10). Graphs show CD52 (left panel), CD84 (middle panel) or PTGER2 (right panel)  $\Delta$  MFI values. Each symbol stands for a single donor sample. \*\*p < 0.01; \*\*\*p < 0.001; \*\*\*\*p < 0.0001, by Friedman test followed by Dunn's multiple comparison test. (B) After gating

on CD66b<sup>+</sup>CD10<sup>+</sup>CD11b<sup>high</sup>CD16<sup>high</sup> mLDNs/mNDNs from GDs (panel I, top and middle panel rows) or mNDNs from HDs (panel I, bottom panel row), CD52<sup>+</sup>PTGER2<sup>+</sup> (II) and CD84<sup>+</sup> (III) cells were identified and overlayed (IV). The frequency of CD52<sup>+</sup>PTGER2<sup>+</sup>CD84<sup>+</sup> mLDNs/mNDNs from GDs (panel IV, top and middle panel rows) and mNDNs from HDs (panel IV, bottom panel row) is reported. One representative experiment for the GD cohort is shown. **(C–D)** Frequency of total CD66b<sup>+</sup> PMN-MDSCs within CD45<sup>+</sup> PBMCs from NSCLC **(C)** or HNC **(D)** patients before (t0) and post (post - therapy) treatment. \*\*\*\*p < 0.0001, by Wilcoxon matched-pairs signed rank test.



**Table S1: Characteristics of HDs, GDs and NSCLC or HNC patients<sup>f</sup>, related to STAR Methods.**

HD <sup>a</sup> donor cohort			GD <sup>b</sup> donor cohort		
Characteristics	n.	%	Characteristics	n.	%
<b>All subjects</b>	51	100	<b>All subjects</b>	27	100
<b>Gender/Age</b>			<b>Gender/Age</b>		
Male	28	55	Male	19	70
Female	23	45	Female	8	30
Male mean age	55 +/- 14.1		Male mean age	34 +/- 11.2	
Female mean age	56 +/- 15.1		Female mean age	39 +/- 13.4	
<b>Cellular sample type</b>					
Bone marrow	10	20			
Peripheral blood	41	80			
NSCLC <sup>c</sup> donor cohort			HNC <sup>d</sup> donor cohort		
Characteristics	n.	%	Characteristics	n.	%
<b>All subjects</b>	29	100	<b>All subjects</b>	65	100
<b>Gender/Age</b>			<b>Gender/Age</b>		
Male	19	66	Male	46	70.1
Female	10	34	Female	19	29.9
Male mean age	71 +/- 5.7		Male mean age	65 +/- 8.8	
Female mean age	69 +/- 8.1		Female mean age	61 +/- 9.2	
<b>Tumor Type</b>			<b>Tumor localization</b>		
Adenocarcinoma	20	69	Oropharynx	34	52
Squamous cell carcinoma	7	24	Oral cavity	9	14
Poorly differentiated NSCLC	2	7	Larynx	19	29
<b>Stage</b>			Hypopharynx	3	5
IA	0	0	<b>T category</b>		
IIA	0	0	T1	20	31
IIIA	3	10	T2	20	31
IVA	9	32	T3	10	15
IB	3	10	T4	15	23
IIB	0	0	<b>Lymph node involvement</b>		
IIIB	3	10	N0	40	62
IVB	11	38	N1	9	14
			N2abc	13	20
			N3	3	5
			<b>Distant metastasis</b>		
			M0	63	97
			M1	2	3
			<b>HPV<sup>e</sup> status of oropharyngeal cancer</b>		
			HPV16 pos	13	38
			HPV16 neg	17	50
			unknown	4	12

<sup>a</sup>HD, healthy donor; <sup>b</sup>GD, G-CSF-treated healthy donor; <sup>c</sup>NSCLC, non-small cell lung cancer; <sup>d</sup>HNC, head and neck cancer; <sup>e</sup>HPV, human papillomavirus; <sup>f</sup>samples utilized for both transcriptomic and flow cytometry experiments.

**Table S2: Characteristics of RCC, TCC, BC and DLBCL patients<sup>c</sup>, related to STAR Methods**

RCC <sup>a</sup> donor cohort			TCC <sup>b</sup> donor cohort		
Characteristics	n.	%	Characteristics	n.	%
<b>All subjects</b>	11	100	<b>All subjects</b>	13	100
<b>Gender/Age</b>			<b>Gender/Age</b>		
Male	10	91	Male	10	77
Female	1	9	Female	3	23
Male mean age	60 +/- 12		Male mean age	68 +/- 14.0	
Female mean age	82		Female mean age	66 +/- 6.7	
<b>Tumor type</b>			<b>T category</b>		
Clear cell RCC	7	64	Ta	10	77
Papillary RCC	3	27	T1	2	15
Chromophobe	1	9	T2	0	0
<b>T category</b>			T3	0	0
T1	4	36	T4	0	0
T2	1	9	Tcis	1	8
T3	5	45	<b>Tumor Grade</b>		
T4	1	9	Low	9	69
<b>Lymph node involvement</b>			High	4	31
N0	6	55	<b>Diagnosis</b>		
N1	2	18	First	7	54
N2	1	9	Recurrent	6	46
Nx	2	18			
<b>Distant metastasis</b>					
M0	11	100			
Mx	0	0			
BC <sup>c</sup> donor cohort			DLBCL <sup>d</sup> donor cohort		
Characteristics	n.	%	Characteristics	n.	%
<b>All subjects</b>	8	100	<b>All subjects</b>	4	100
<b>Gender/Age</b>			<b>Gender/Age</b>		
Male	0	0	Male	1	25
Female	8	100	Female	3	75
Male mean age			Male mean age	76	
Female mean age	72 +/- 5.9		Female mean age	62 +/- 10.1	
<b>Tumor type</b>			<b>Stage (Ann Arbor)</b>		
Lobular	2	25	II	1	25
Ductal	4	50	III	2	50
Lobular and Ductal	2	25	IV	1	25
<b>Stage</b>					
IV	8	100			

<sup>a</sup>RCC, renal cell carcinoma; <sup>b</sup>TCC, transitional cell carcinoma; <sup>c</sup>BC, breast cancer; <sup>d</sup>DLBCL, diffuse large B cell lymphoma; <sup>e</sup>blood samples utilized for flow cytometry experiments.

## SUPPLEMENTAL REFERENCES

- S1. Salcher, S., Sturm, G., Horvath, L., Untergasser, G., Kuempers, C., Fotakis, G., Panizzolo, E., Martowicz, A., Trebo, M., Pall, G., et al. (2022). High-resolution single-cell atlas reveals diversity and plasticity of tissue-resident neutrophils in non-small cell lung cancer. *Cancer Cell*. 10.1016/j.ccell.2022.10.008
- S2. Zilionis, R., Engblom, C., Pfirschke, C., Savova, V., Zemmour, D., Saatcioglu, H.D., Krishnan, I., Maroni, G., Meyerovitz, C.V., Kerwin, C.M., et al. (2019). Single-Cell Transcriptomics of Human and Mouse Lung Cancers Reveals Conserved Myeloid Populations across Individuals and Species. *Immunity*. 50, 1317-1334 e1310. 10.1016/j.immuni.2019.03.009
- S3. Grassi, L., Pourfarzad, F., Ullrich, S., Merkel, A., Were, F., Carrillo-de-Santa-Pau, E., Yi, G., Hiemstra, I.H., Tool, A.T.J., Mul, E., et al. (2018). Dynamics of Transcription Regulation in Human Bone Marrow Myeloid Differentiation to Mature Blood Neutrophils. *Cell. Rep*. 24, 2784-2794. 10.1016/j.celrep.2018.08.018
- S4. Condamine, T., Dominguez, G.A., Youn, J.I., Kossenkova, A.V., Mony, S., Alicea-Torres, K., Tcyganov, E., Hashimoto, A., Nefedova, Y., Lin, C., et al. (2016). Lectin-type oxidized LDL receptor-1 distinguishes population of human polymorphonuclear myeloid-derived suppressor cells in cancer patients. *Sci. Immunol*. 1. 10.1126/sciimmunol.aaf8943
- S5. Mistry, P., Nakabo, S., O'Neil, L., Goel, R.R., Jiang, K., Carmona-Rivera, C., Gupta, S., Chan, D.W., Carlucci, P.M., Wang, X., et al. (2019). Transcriptomic, epigenetic, and functional analyses implicate neutrophil diversity in the pathogenesis of systemic lupus erythematosus. *Proc. Natl. Acad. Sci U. S. A*. 116, 25222-25228. 10.1073/pnas.1908576116
- S6. Pillay, J., Kamp, V.M., van Hoffen, E., Visser, T., Tak, T., Lammers, J.W., Ulfman, L.H., Leenen, L.P., Pickkers, P., Koenderman, L. (2012). A subset of neutrophils in human systemic inflammation inhibits T cell responses through Mac-1. *J. Clin. Invest*. 122, 327-336. 10.1172/JCI57990
- S7. Calzetti, F., Finotti, G., Tamassia, N., Bianchetto-Aguilera, F., Castellucci, M., Cane, S., Lonardi, S., Cavallini, C., Matte, A., Gasperini, S., et al. (2022). CD66b(-)CD64(dim)CD115(-) cells in the human bone marrow represent neutrophil-committed progenitors. *Nat. Immunol*. 10.1038/s41590-022-01189-z